Western Boundary Current in relation to Atlantic Subtropical Gyre dynamics during abrupt glacial climate fluctuations

Dirk Nürnberg[1], Tabitha Riff[1], André Bahr[2], Cyrus Karas[3], Karl Meier[2], Jörg Lippold[2]

[1]GEOMAR Helmholtz Centre for Ocean Research Kiel, Wischhofstr. 1-3, D-24148 Kiel, Germany

[2]Institute of Earth Science, Heidelberg University, Im Neuenheimer Feld 234, D-69120 Heidelberg, Germany

[3]Universidad de Santiago, Av. B. O'Higgins 3363, Santiago, Chile

Correspondence to: Dirk Nürnberg (dnuernberg@geomar.de)

Abstract (236 words)

Ocean-atmosphere simulations corroborate the relationship between tropical Atlantic subsurface heat and salt storage driven by Salinity Maximum Water (SMW) and deglacial perturbations of the Atlantic Meridional Overturning Circulation (AMOC). Whether AMOC variability of the last glacial cycle affected SMW export into the tropical West Atlantic remained yet elusive. In order to assess the sensitivity of the tropical hydrography during abrupt and rapid glacial climatic and oceanic perturbations, we present century-resolving foraminifera-based subsurface (~200m water depth) temperature and salinity reconstructions from Tobago Basin core M78/1-235-1. The proxy records were interpreted in terms of the closely related development of the North Brazil Current (NBC) and the North Atlantic Subtropical Gyre (STG) from ~37 to 30 ka BP, and in relation to their deglacial developments. Prior to ~32.8 ka BP, the cyclic variations in subsurface conditions were attributed to the NBC, which acted in line with a recurrent intensification and relaxation of the trade winds, subtle migrations of the Intertropical Convergence Zone, and the related moisture transport across Central America. Major and rapid re-organizations of the tropical Atlantic upper ocean-atmosphere system took place at ~32.8 ka BP and ~21.8 ka BP,

unmirrored by major AMOC changes. Thresholds for sufficient heat and salinity accumulation in the STG to allow for formation and intensified subsurface dispersal of SMW were not achieved before late HS1, when AMOC weakening, according tropical heat backlog and surface warming by maximum Northern Hemisphere insolation acted together.

Keywords: North Brazil Current, Atlantic Subtropical Gyre, Abrupt Climate Change, Foraminiferal Geochemistry

1. Introduction

The Atlantic Meridional Overturning Circulation (AMOC) is responsible for the global distribution of heat, salt, moisture, CO_2, and nutrients and hence, its temporal and spatial variability is highly relevant to the global climate system (e.g. Buckley and Marshall, 2016). Modelling studies and oceanographic data point to a close coupling between the strength of the AMOC and the dynamics of both the North Atlantic Subtropical Gyre (STG) and the Subpolar Gyre (SPG) . The coupling between the tropical Atlantic and the high-latitude North Atlantic via northward flowing warm and saline waters (the Atlantic Inflow) is likely preconditioned by intensified evaporation in the STG area on longer time scales (Hátún et al., 2005) with stabilizing effects on the THC (e.g. Latif et al., 2000). On interannual to inter-decadal time scales, however, it is primarily the dynamics of the SPG circulation and its effects on the location, intensity, and composition of the North Atlantic Current in the northeastern Atlantic, which drives the Atlantic Inflow (Hátún et al., 2005). It is enhanced when atmospheric forcing, i.e. the amplitude of the wind stress curl, is weaker than normal. Then, both the STG and SPG weaken and the Polar Front moves westward, opening the pathway for subtropical waters to enter the eastern boundary current (Häkkinen et al., 2011). As a large reservoir for ocean heat and salt (Schmitz and McCartney, 1993), the predominantly wind-driven STG is critical to the upper ocean circulation, and reacts sensitively to climatic variations. The close interrelationship between oceanic and atmospheric processes affects the STG circulation, and the formation of Salinity Maximum Water (SMW) related to strengthened Ekman pumping (Slowey and Curry, 1995).

The impact of glacial and deglacial climatic changes on the STG variability and the spread of SMW is a matter of debate. Several proxy records point to the southward displacement of the northern boundary of the STG during North Atlantic cold spells (Calvo et al., 2001; Repschläger et al., 2015; Schwab et al., 2012) synchronous to the presumably weakened AMOC during Heinrich Stadials HS2 (27–24 ka BP; Stern and Lisiecki, 2013), HS1 (18–14.6 ka BP; Barker and Diz, 2014), and the Younger Dryas (YD, 12.8–11.5 ka BP; Barker and Diz, 2014). At the southern margin of the STG, the sluggish AMOC circulation and the southward displaced Intertropical Convergence Zone (ITCZ) likely weakened the Western Boundary Current (WBC) system. Modelling studies suggest that the WBC decline causes horizontal ocean heat advection at subsurface near the southern boundary of the STG (Chang et al., 2008). When the AMOC weakens to the point when its northwestward return flow strength is overcome by its equatorward flowing branch, the North Brazil Current (NBC; c.f. Fig. 1E) even reverses its direction, thereby opening the pathway of warmer/saltier STG water to enter the equatorial ocean areas (Chang et al., 2008). According to the simulations of Chang et al. (2008), the warm anomaly excites equatorial Kelvin waves once it is advected close enough to the equator. These transport the warm anomaly eastward along the equator and then poleward along the eastern boundaries. Subsurface temperature reconstructions from the tropical West Atlantic (Reißig et al., 2019; Schmidt et al., 2012) substantiate the modeling results and prove substantial subsurface warming during deglacial AMOC perturbations. The documented sensitivity of the STG to deglacial AMOC perturbations raises the question if and how associated changes in the (sub)tropical heat and salt budget could have altered AMOC strength itself.

By complementing and combining subsurface temperature and salinity records from a key oceanographic location in the tropical West Atlantic (Tobago Basin, Fig. 1), we provide new aspects on the functioning of the WBC and the SMW in relation to the stadial/interstadial Dansgaard-Oeschger (D/O) climate variability (Marine Isotope Stage MIS3), and set them in relation to the deglacial to early Holocene development (Reißig et al., 2019). The new proxy data series based on the subsurface (~200 m water depth) dwelling species *Globorotalia truncatulinoides* from sediment core M78/1-235-1 (Fig. 1) are compared to similar proxy data from adjacent Bonaire Basin (Parker et al., 2015; Schmidt et al., 2012) and other reference sites. We address the questions: How and why did the thermal structure of the tropical West Atlantic change during the last glacial in relation to the subsequent deglaciation? How was this change related to ocean and climate dynamics in the higher latitude northern and southern Atlantic areas?

2. Regional setting

The Tobago Basin is located in the tropical West Atlantic close to the Grenada Passage, which shows the largest average water transport of tropical Atlantic surface and deep water (~5.7 Sv; 1 Sverdrup = $10^6 m^3 s^{-1}$) through the Lesser Antilles into the Caribbean (Johns et al., 2002) (Fig. 1). The Tobago Basin is at the mixing zone of warm and high saline subsurface waters of the STG, the related SMW, and the northbound NBC (Fig. 1B). The subsurface waters in Tobago Basin are mainly affected by the northward flowing WBC system, which transports water mainly in the upper 150 m, driven partly by wind, partly by the thermohaline circulation (Johns et al., 2002). The NBC is part of this current system and dependent on the season provides either a conduit for cross-equatorial transport of upper-ocean waters as part of the AMOC, or closes the wind-driven equatorial gyre circulation, and as such feeds a system of zonal countercurrents (Johns et al., 2002).

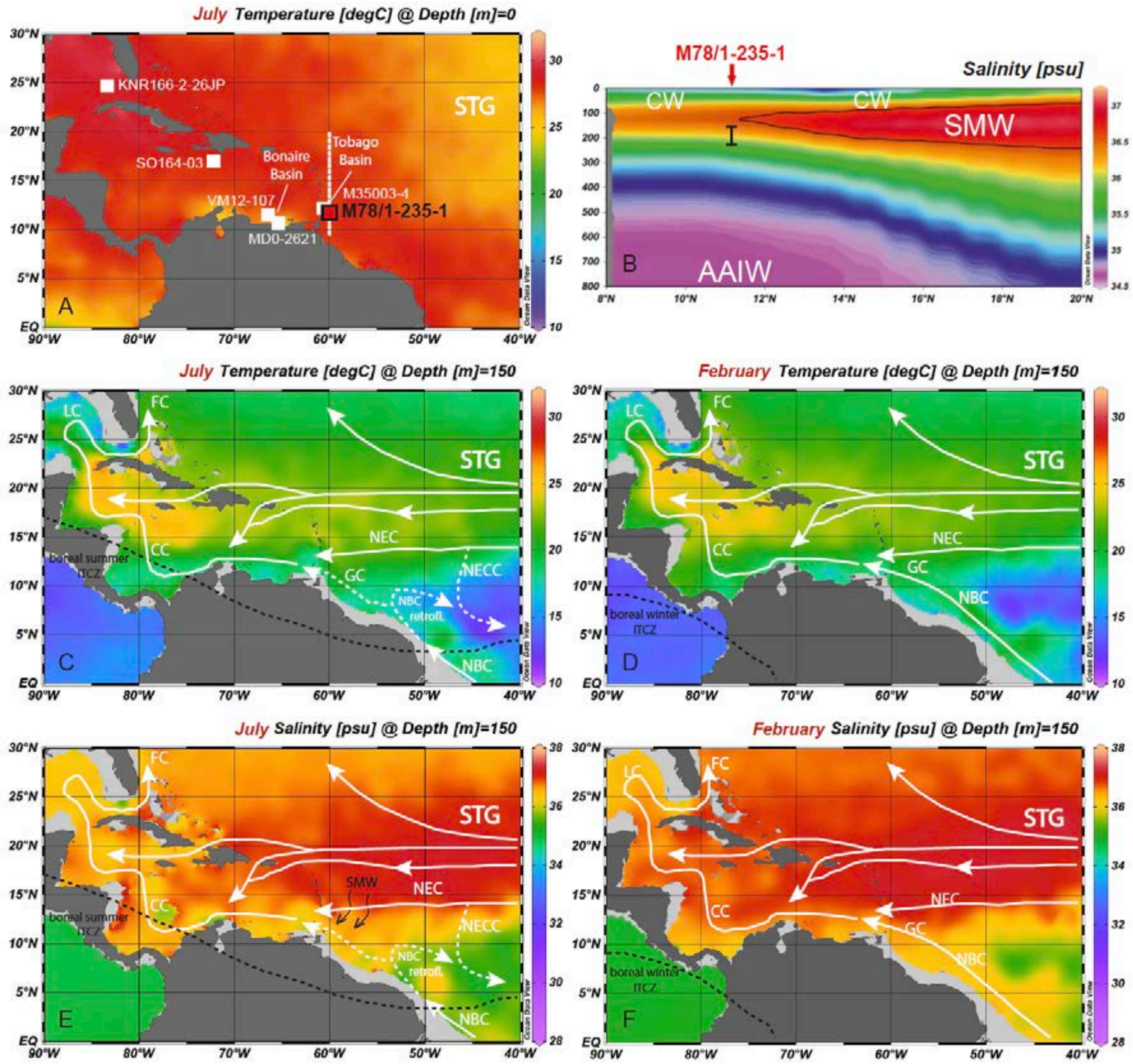

Fig. 1. Tropical West Atlantic surface and subsurface hydrological setting. A) Sea surface boreal summer temperatures at 0 m water depth. Locations of proxy records discussed are included. Red square: core M78/1-235-1, termed 235, Tobago Basin (this study). White squares: reference sites VM12-107, termed 107, Bonaire Basin (Parker et al., 2015; Schmidt et al., 2012); M35003-4, Tobago Basin (Zahn and Stüber, 2002); SO164-03, Beata Ridge (Reißig et al., 2019); KNR166-2-26JPC, Florida Straits (Lynch-Stieglitz et al., 2014); MD03-2621, Cariaco Basin (Deplazes et al., 2013). **B)** Annual salinity profile from 8°N to 20°N, along dotted white line in A). The black isoline marks the SMW with >36.5 salinity [psu]. Black vertical bar denotes the assumed living depth of the foraminiferal species (*G. truncatulinoides*) studied here. **C)** Boreal summer temperatures at 150 m water depth. **D)** Boreal winter temperatures at 150 m water depth. **E)** Boreal summer salinity at 150 m water depth. **F)** Boreal winter salinity at 150 m water depth. White arrows and dashed lines mark modern, seasonally varying surface to subsurface currents. Black dashed lines depict boreal summer and winter positions of the ITCZ. AAIW: Antarctic Intermediate Water; CC: Caribbean Current; CW: Caribbean Water; FC: Florida Current; GC: Guyana Current; LC: Loop Current; NBC: North Brazil Current; NEC: Northern Equatorial Current; NECC: Northern Equatorial Counter Current; SMW: Salinity Maximum Water; STG: Subtropical Gyre. Maps created with Ocean Data View (Schlitzer, 2015) based on hydrographic data from Locarnini et al. (2013).

Highest NBC transport (cooler/fresher) is during boreal summer/fall, in line with strengthened trade winds and the northernmost position of the ITCZ located at the southern edge of the Caribbean (6–10°N) (Philander and Pacanowski, 1986). Concurrently, waters from the NBC mixing with strengthened Amazon River discharge are eastward retroflected into the North Equatorial Countercurrent (NECC) (Hu et al., 2004; Johns et al., 2002), leading to a weaker Guyana Current (GC) and, in combination with the weaker northeastern trade winds, a less strong Caribbean Current (CC) (Hu et al., 2004; Vellinga and Wu, 2004). Thereby, the NBC remains significantly cooler and fresher (<18°C; <37 [psu]) than SMW formed in the STG further to the north (Drijfhout and Hazeleger, 2006; Fratantoni et al., 2000; Kirchner et al., 2009) (Fig. 1D, c.f. Appendix Fig. A.1). During boreal winter/spring, the NBC in combination with the North Equatorial Current (NEC) contributes to the GC and the CC entering the southern Caribbean Sea (Hellweger and Gordon, 2002; Kameo et al., 2004). At the same time, the ITCZ reaches its most southerly position (0–5°S), northeastern trade winds reach their maximum strength (Philander and Pacanowski, 1986), and the by-volume largest westward surface flow of the CC occurs. The enhanced westward wind stress causes pronounced coastal upwelling along the continental margin of South America. At 80-180 m water depth, the high-saline (salinity >36.5 [psu]) SMW (often termed Subtropical Under Water) (Kameo et al., 2004) is present with annual subsurface temperatures of ~17°C (Locarnini et al., 2018; c.f. Appendix Fig. A.1). The SMW originates in the central North Atlantic, in the northwestern part of the STG, where evaporation exceeds precipitation (Hernández-Guerra and Joyce, 2000; O'Connor et al., 2005). Here, surface water is subducted through Ekman-downwelling associated to trade wind activity into the salinity maximum zone (Qu et al., 2013). These processes promote both the formation and the southward spread of warm and saline SMW into the subtropical shallower circulation cell via the NEC (e.g. Blanke, 2002) and changes the subsurface properties in the tropical

Atlantic (e.g. Mignot et al., 2007). Together, Caribbean Water (CW) and SMW form the permanent Caribbean thermocline, which separates warm surface waters from underlying cooler waters (Wüst, 1964). The northward flowing western boundary NBC interacts with the NEC, separating SMW from fresher and cooler subsurface waters of the NBC at ~10°N (e.g. Drijfhout and Hazeleger, 2006). Today, SMW does not significantly affect the Tobago and Bonaire basins, as weak northeastern trade winds, the northern position of the ITCZ, and a strong NBC keep the warm/salty waters of the STG north of ~10°N, and allow northward flowing cooler/fresher tropical waters to enter the southern Caribbean (e.g. Drijfhout and Hazeleger, 2006) (Fig. 1D).

3. Material and methods

3.1 Sampling

During R/V Meteor Cruise 78/1 (Schönfeld et al., 2011), piston core M78/1-235-1 (hereafter referred to as core 235) was recovered from Tobago Basin (11°36.53´N 60°57.86´W) from 852 m water depth, which is in the core depth of Antarctic Intermediate Water (AAIW). At surface and subsurface, the core site is within the mixing zone of SMW and NBC water (Fig. 1B, D). The sediments of Tobago Basin are mainly of olive-gray to light greenish-gray sandy silty clay with common bioturbation, deposited below suboxic waters. Various paleoceanographic proxy data and interpretations are already available from this core, discussing last deglacial to Holocene oceanographic variability at surface (Bahr et al., 2018; Hoffmann et al., 2014), at subsurface (Reißig et al., 2019), and at intermediate water depths (Poggemann et al., 2017, 2018). This study extends the existing subsurface proxy records further back in time, now focusing on the time period of the latest fully developed D/O events (~30-37 ka BP). Sampling and analytical studies were carried out from 630 to 800 cm core depth at 1 cm-spatial resolution.

3.2 Chronostratigraphy

For the time period 0-24 ka BP, the chronostratigraphy of core 235 was initially published by Hoffmann et al. (2014) and Poggemann et al. (2017; 2018), and extended down to 30 ka BP by Reißig et al. (2019). We here updated and prolonged the chronostratigraphy down to ~37 ka BP by adding new Accelerator Mass Spectrometry (AMS) radiocarbon (^{14}C) datings and by fine-tuning the proxy records to climate reference records at high-resolution. The age model is primarily based on the linear interpolation between 12 AMS^{14}C datings (Fig. 2; c.f. Appendix Tab. A.1). For AMS^{14}C dating, a mix of shallow-dwelling planktonic foraminiferal tests (*Globigerinoides ruber* and *Globigerinoides sacculifer*) was selected. Due to insufficient sample material at 628 cm core depth, specimens of *Orbulina universa* were added here. All AMS^{14}C dates were calibrated applying the Calib7.1 software (Stuiver et al., 2020; http://calib.org), using the MARINE20 database. This resulted in AMS^{14}C ages being slightly different from those used in the previous age model (e.g. Reißig et al., 2019) still based on MARINE13 (c.f. Appendix Tab. A.1). The marine calibration incorporates a time-dependent global ocean reservoir correction of ~550 years, which broadly corresponds to Sarnthein et al. (2015), who defined reservoir ages spanning from ~700 to ~25 ^{14}C years in the tropical West Atlantic during the LGM and the deglaciation. To account for local effects, the difference ΔR in reservoir age of the tropical West Atlantic/Caribbean and the model ocean was additionally considered. The Calib7.1 marine reservoir correction database provides a ΔR-value of -161 $\pm$ 24 years derived from a SW Puerto Rican massive coral (c.f. Kilbourne et al., 2007), which traces subtropical and equatorial water mixing similarly as our site location.

The AMS^{14}C constraints produce a convincing linear correlation (= 0.8) of the benthic $\delta^{18}O_{Uvigerina}$ record to the Antarctic EDML $\delta^{18}O$ record (EPICA Community Members, 2006) (Fig. 2B). This good match is basically expected as core 235 is from 852 m water depth in the core of modern AAIW originating from the Southern Ocean. It is striking, however, that the benthic $\delta^{18}O_{Uvigerina}$ record exhibits rapid and high-amplitude variations in particular during the last deglaciation, reminiscent of the typical deglacial northern hemisphere climate pattern. The AMS^{14}C constraints place prominent intermediate-depth benthic $\delta^{18}O_{Uvigerina}$ minima to the deglacial cool periods (early) HS 1 and the Younger Dryas (YD) (Fig. 2B, green shadings; c.f. Appendix Tab. A.1), an observation similarly made in the intermediate-depth tropical West Atlantic by Hüls and Zahn (2000), Rühlemann et al. (2004), and Pahnke et al. (2008). The exceptionally light benthic $\delta^{18}O_{Uvigerina}$ values during these cool climate phases are likely due to intermediate depth warming evidenced by $Mg/Ca_{Uvigerina}$-based temperature reconstructions on the same core 235 (Poggemann et al., 2018). According to Poggemann et al. (2018) the deglacial AMOC slowdowns caused the accumulation of ocean warmth in the Southern Ocean, which then is transported northward at intermediate depths via AAIW. Under the constraints of radiocarbon dates within their calculated 1-σ errors, further benthic $\delta^{18}O_{Uvigerina}$ minima fall into Greenland stadials GS-8 and GS-6 (Fig. 2B, green shadings; c.f. Appendix Tab. A.1). Following this AMS^{14}C-constrained pattern of benthic $\delta^{18}O_{Uvigerina}$ minima during stadials and deglacial cool periods, we placed 2 additional tielines in order to yield an optimized match of the benthic $\delta^{18}O_{Uvigerina}$ minima and the cool periods GS-7 and GS-5 (Fig. 2B, green stippled lines; c.f. Appendix Tab. A.1) using the software AnalySeries (Paillard et al., 1996). These tielines were set in order to sharpen the stadial-interstadial pattern of the $\delta^{18}O_{Uvigerina}$ record. They move the initial ages based on the AMS^{14}C-ages by not more than 100 years towards the younger.

The chronostratigraphic framework of core 235 is verified in particular in the older section >32.8 ka BP by the fact that the upper ocean proxy parameters reveal a robust cyclicity related to the northern hemisphere climate pattern (see discussion and Fig. 4B). The age model is further supported by the covariance between the highly variable core 235 optical sediment lightness (L*)-record and the well-dated L*-record of nearby core MD03-2621 from Cariaco Basin (Deplazes et al., 2013), relating L* maxima predominantly to cool (glacial and stadial) periods (Fig. 2C). Both records reflect the short-term variability of the tropical climate system, with low L* pointing to high terrigenous riverine input diluting the biogenic carbonate content (c.f. Hoffmann et al., 2014).

Our chronostratigraphical approach led us to exclude 2 AMS^{14}C-dates from our age calculations (c.f. Appendix Tab. A.1). The rejected AMS^{14}C-date at 316.5 cm provides an age of ~14.9 ka BP, which appears too young by several hundreds of years in view of the consecutive age increase of the surrounding AMS^{14}C-dates. Its 1-σ error largely overlaps with the 1-σ-error of the shallower (298 cm; ~15.1 ka BP) AMS^{14}C-date (c.f. Appendix Tab. A.1). Both AMS^{14}C-dates are within AMS^{14}C-plateau 1 (defined by Sarnthein et al., 2019 to ~14.2-15.2 ka BP), which illustrates the potential stratigraphical uncertainty of the radiocarbon dating technique (Fig. 2A). We hence find it justified not to consider the abovementioned dating. Similarly, we removed the AMS^{14}C-dates at 762 cm core depth, which provides an age of ~33.7 ka BP being rather similar (within the 2-σ error) to the AMS^{14}C-dating from ~60 cm further above. To test the robustness of the chronostratigraphy, we modelled the age-depth relation using the CRAN R package Bacon (version 2.5.1) (Blaauw and Christen, 2011). All AMS^{14}C dates and the local reservoir effect of $\Delta R = -161 \pm 24$ years were considered in the model approach based on R-Bacon. The model output indicates that the two AMS^{14}C dates at 316.5 cm and 762 cm were not within the probability-range reconstructed by R-Bacon (Fig. 2A). The R-Bacon script uses a Student-t model to calibrate AMS^{14}C dates with wider tails of the calibration model making it more robust to outlying AMS^{14}C dates (Blaauw and Christen, 2011). Sedimentation rates calculated in the base of this age model average to ~30 cm/kyr, with maxima during the warm B/A and GI-6 and GI-7 time periods (Fig. 2D).

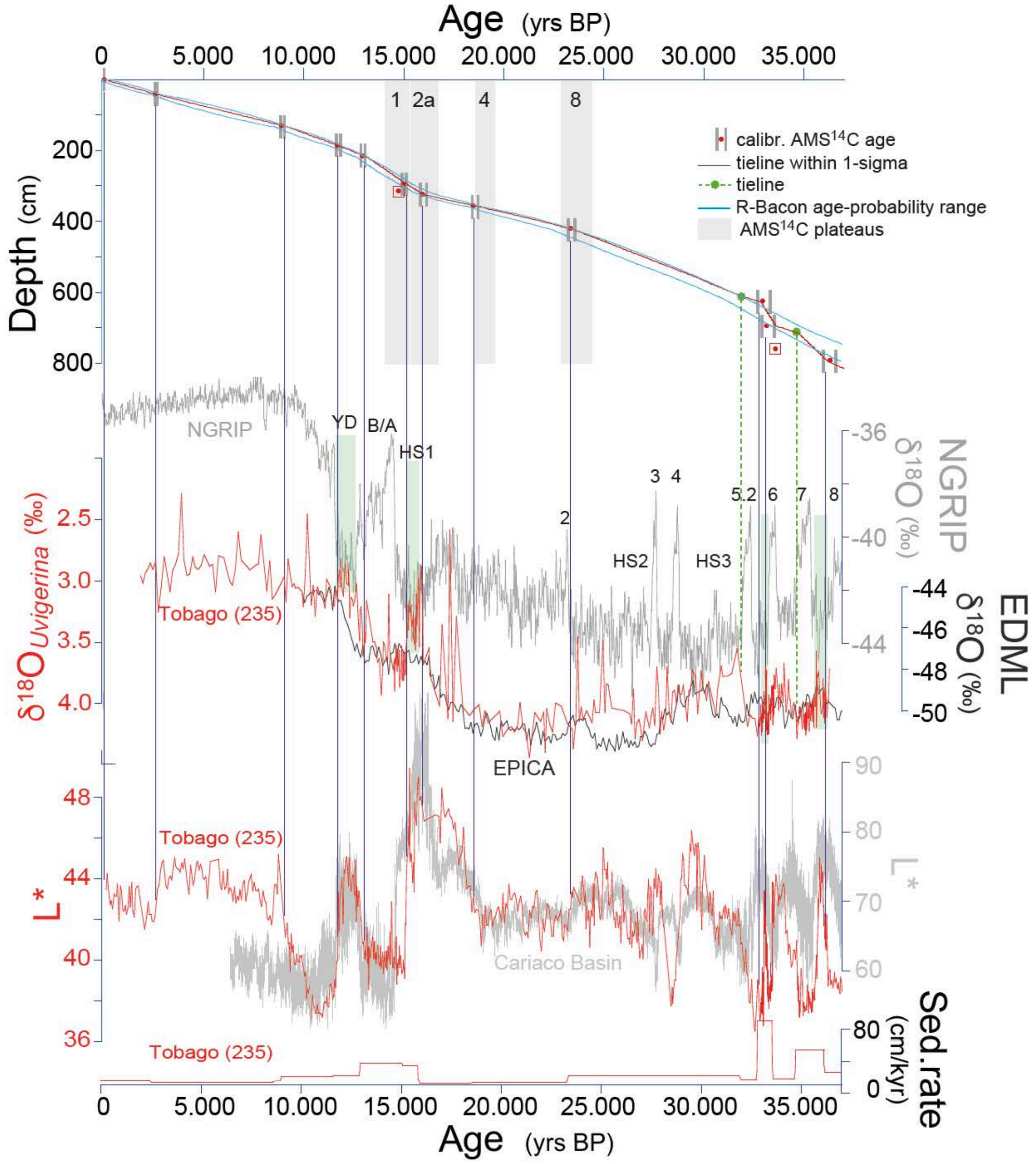

Fig. 2. Chronostratigraphy of sediment core M78/1-235-1. A) Depth-age diagram based on AMS^{14}C-datings (red dots including gray 1-σ error bars) and additional tie lines (green dots and green stippled lines) (c.f. Appendix Tab. A.1). Rectangled red dots = rejected. Gray shading areas mark AMS^{14}C plateaus 1, 2a, 4 and 6 (Sarnthein et al., 2019) in order to illustrate the potential stratigraphical uncertainty of 4 AMS^{14}C-datings. The R-Bacon age-probability range is included (Blaauw and Christen, 2011). **B)** The benthic δ^{18}O record of Tobago Basin core 235 (red; ‰ VPDB) in comparison to the northern (NGRIP Dating Group, 2006; gray; ‰ SMOW) and the southern hemisphere δ^{18}O reference records (EPICA Group Members, 2006, black; ‰ SMOW) based on i) AMS^{14}C-datings (blue lines placed within the 1-σ error) and ii) 2 tie lines (green stippled lines). Green shadings mark light benthic δ^{18}O$_{Uvigerina}$ excursions related to deglacial (HS1 = Heinrich Stadial 1; YD = Younger Dryas) and cool Greenland stadials GS-8 and GS-6. **C)** Resulting sediment reflectance (L*) record of core 235 (red) in comparison to reference core MD03-2621 (Cariaco Basin; Deplazes et al., 2013; gray; c.f. Fig. 1A). **D)** Resulting 5-point smoothed sedimentation rates of core 235. B/A = Bølling/Allerød (14.6–12.8 ka).

3.3 Foraminiferal geochemistry

Subsurface conditions were approximated from (isotope-)geochemical parameters measured within the calcitic tests of the deep-dwelling planktonic foraminiferal species *Globorotalia truncatulinoides* (d´Orbigny, 1839) (Lohmann and Schweitzer, 1990). In agreement with the findings of Jentzen et al. (2018b) from the eastern Caribbean and as the majority of the *G. truncatulinoides* specimens in core 235 were encrusted (c.f. Appendix Fig. A.2), we assume a habitat depth range of ~200-250 m (detailed discussion in Appendix Text A.1). This corresponds to a depth nearly below the main thermocline in Tobago Basin (180-220 m) (Locarnini et al., 2018; c.f. Appendix Fig. A.1). We routinely selected 30-40 specimens per sample from the size fraction 355-400 µm. In a few cases, the size fraction was enlarged to 250-400 µm due to insufficient sample material. The foraminiferal tests were cracked between cleaned glass plates to open the chambers for efficient subsequent cleaning. One third of the fragments were used for stable isotope analyses, the remaining two thirds for trace metal analyses (detailed discussion in Appendix Text A.1).

3.3.1 Foraminiferal stable oxygen isotopes

Stable oxygen ($\delta^{18}O$) (c.f. Appendix Fig. A.6) isotope analyses were performed on a Thermo Scientific MAT 253 mass spectrometer with an automated Kiel IV Carbonate Preparation Device at GEOMAR. The isotope values were calibrated versus the NBS19 (National Bureau of standards) carbonate standard and an in-house standard ("Standard Bremen"). Isotope values presented in the delta-notation are reported in permille (‰) relative to the VPDB (Vienna Peedee Belemnite) scale. The long-term analytic precision is 0.06 ‰ for $\delta^{18}O$ and 0.03 ‰ for $\delta^{13}C$. The revealed $\delta^{18}O$ reproducibility of 148 measurements of *G. truncatulinoides* is ± 0.14‰.

3.3.2 Mg/Ca-paleo thermometry

Prior to elemental analyses, the foraminiferal tests were cleaned following the initial cleaning procedures of Boyle and Keigwin (1985/86) and Boyle and Rosenthal (1996). These include both oxidative and reductive (with hydrazine) cleaning steps. This procedure was similarly applied by Reißig et al. (2019) on core 235 foraminiferal sample material, and allows direct comparison of analytical results (c.f. Appendix A.1). Trace metal analyses were performed on a VARIAN 720-ES Axial ICP-OES, a simultaneous, axial-viewing Inductively Coupled Plasma - Optical Emission Spectrometer coupled to a VARIAN SPS3 sample preparation system. To assure analytical quality control the measurement strategy involved the regular analyses of standards and blanks. The results were normalized to the ECRM 752-1 standard (3.761 mmol/mol Mg/Ca; Greaves et al., 2008) and were drift corrected. The external reproducibility for the ECRM standard was ±0.01 mmol/mol for Mg/Ca (2σ standard deviation). Replicate measurements reveal a reproducibility of ±0.28 mmol/mol for *G. truncatulinoides* (2σ). See Appendix (c.f. Appendix A.1; Figs. A.4, A.5) for further details and information on contamination and dissolution issues.

The $Mg/Ca_{G.truncatulinoides}$ ratios were converted into subsurface temperatures (termed $subSST_{Mg/Ca}$ in the following) using the species-specific exponential calibration equation of Cléroux et al. (2008) established from widely distributed Atlantic sample material (c.f. Appendix Fig. A.3). For consistency, reference planktonic Mg/Ca data sets (in particular Parker et al., 2015; Schmidt et al., 2012) were translated into temperatures using the above-mentioned calibration.

3.3.3 Oxygen isotope signature of seawater approximating paleo salinity

In the upper ~600 m of the Caribbean, modern $\delta^{18}O_{sw}$ and salinity are linearly correlated ($\delta^{18}O_{sw} = 0.36 * S - 12.31$; $R = 0.84$; Schmidt et al., 1999; $\delta^{18}O_{sw} = 0.35 * S - 11.78$;

R = 0.81; Jentzen et al., 2018a). Past local salinity variations at subsurface depths were approximated from $\delta^{18}O_{sw}$ derived from combined planktonic foraminiferal $\delta^{18}O$ and $subSST_{Mg/Ca}$ (e.g., Nürnberg et al., 2008; 2015). In a first step, the temperature effect was removed from the initial foraminiferal $\delta^{18}O$ by using the temperature versus $\delta^{18}O_{calcite}$ equation of Thunell et al. (1999): $\delta^{18}O_{sw} = (\delta^{18}O_{foram} + 0.27) – 0.2083\ (14.9 - subSST_{Mg/Ca})$. In a second step, we calculated the regional ice-volume-free $\delta^{18}O_{sw}$ record ($\delta^{18}O_{sw\text{-}ivf}$) by accounting for changes in global $\delta^{18}O_{sw}$, which were due to continental ice volume variability. Here, we used the relative sea level reconstruction of Grant et al. (2012) as it offers a high temporal resolution during MIS 3 and times of D/O variability. The propagated 2σ error in $\delta^{18}O_{sw\text{-}ivf}$ is ±1.16 ‰ for *G. truncatulinoides* (c.f. Reißig et al., 2019) and hence, is larger than for the shallow-dweller *G. ruber* (±0.4 ‰; e.g., Bahr et al., 2013). The larger error seems to reflect i) the high biological and hydrographic variability and ii) the comparatively large uncertainty of the Mg/Ca-temperature calibration applied (Cléroux et al., 2008). Nonetheless, the averaged early Holocene (~10.5-7.2 ka BP) $\delta^{18}O_{sw\text{-}ivf}$ value of 1.3 ‰ matches the modern $\delta^{18}O_{sw}$ of 1.2-1.3 ‰ in the eastern Caribbean (Jentzen et al., 2018a; c.f. Figs. 3, 4). The $\delta^{18}O_{sw\text{-}ivf}$ values were not converted into salinity units, as it is not warranted that the modern linear relationship between $\delta^{18}O_{sw}$ and salinity held through time due to changes in the sea ice regime, ocean circulation, and freshwater budget (e.g. Caley and Roche, 2015).

4. Results and discussion

4.1 Tobago Basin subsurface temperatures and salinity approximation

Here, we extended the $subSST_{Mg/Ca}$ and subsurface $\delta^{18}O_{sw\text{-}ivf}$ proxy records of Tobago Basin core 235 (Reißig et al., 2019) from ~30 ka to ~37 ka BP (Fig. 3B-E), thereby setting the deglacial extreme subsurface warming events observed by Reißig et al. (2019) into the broader framework of previous rapid oceanic re-organizations at subsurface. From 37 to 30 ka BP, $\delta^{18}O_{G.truncatulinoides}$ shows an overall range between 0.6 ‰ and 2.9 ‰ with short-term high-amplitude fluctuations of >1 ‰. $Mg/Ca_{G.truncatulinoides}$ ratios vary between 1.63 and 2.59 mmol/mol and show amplitude variations of ~1.2 mmol/mol around a mean of 1.88 mmol/mol. The calculated $subSST_{Mg/Ca}$ range is between ~10°C and ~19°C. The calculated $\delta^{18}O_{sw\text{-}ivc}$ values reflecting subsurface salinity range between ~2.4 ‰ and 0 ‰. After ~32.8 ka BP, our $\delta^{18}O_{G.truncatulinoides}$ record reveals a gradual shift towards heavier values, reaching ~2.2 ‰ during GI-5.1. Similarly, $Mg/Ca_{G.truncatulinoides}$ abruptly increases by ~0.44 mmol/mol at ~32.8 ka BP and remains relatively high between 2 - 2.6 mmol/mol. Although at lower temporal resolution since ~32.8 ka BP (due to lower sampling resolution at lowered sedimentation rates; c.f. Fig. 2), these changes in both $\delta^{18}O_{G.truncatulinoides}$ and $Mg/Ca_{G.truncatulinoides}$ records are significant. The low $Mg/Ca_{G.truncatulinoides}$ values before ~32.8 ka BP are associated with heavier $\delta^{18}O_{G.truncatulinoides}$ values, while such relationship is not apparent afterwards.

347

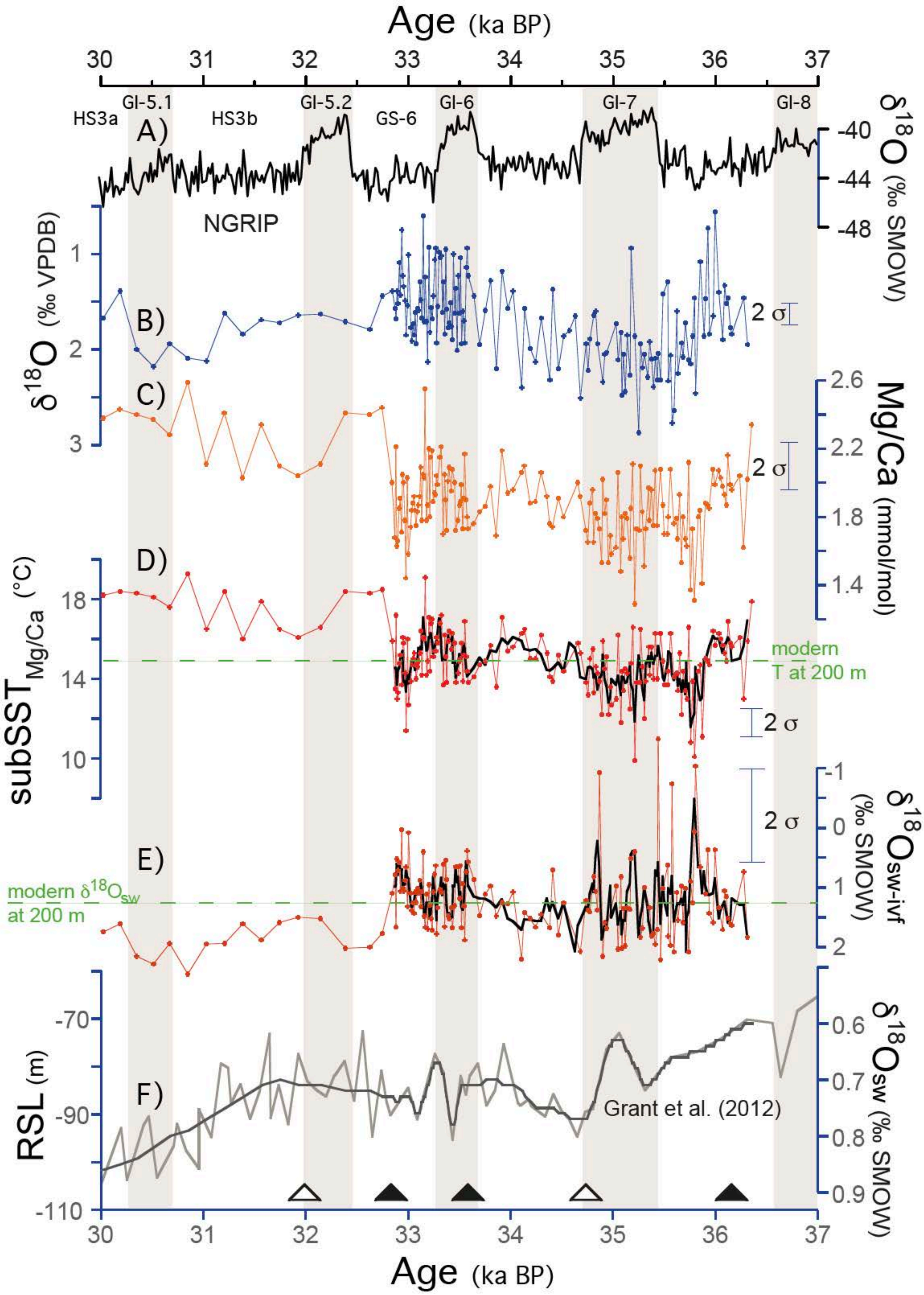

Age (ka BP)
30 31 32 33 34 35 36 37
HS3a
GI-5.1
HS3b
GI-5.2
GS-6
GI-6
GI-7
GI-8
A)
B)
C)
D)
E)
F)
NGRIP
δ18O (‰ SMOW)
-40
-44
-48
δ18O (‰ VPDB)
1
2
3
2 σ
Mg/Ca (mmol/mol)
2.6
2.2
1.8
1.4
subSST Mg/Ca (°C)
18
14
10
modern
T at 200 m
δ18Osw-ivf (‰ SMOW)
-1
0
1
2
modern δ18Osw
at 200 m
RSL (m)
-70
-90
-110
δ18Osw (‰ SMOW)
0.6
0.7
0.8
0.9
Grant et al. (2012)

Fig. 3. Analytical results of *G. truncatulinoides* from Tobago Basin sediment core M78/1-235-1 (this study). **A)** Greenland ice core $\delta^{18}O$ record as reference for the northern hemisphere climate signal (NGRIP Dating Group, 2006). **B)** Stable oxygen isotopes ($\delta^{18}O$). **C)** Mg/Ca ratios. **D)** Calculated subsurface temperatures ($subSST_{Mg/Ca}$; high-resolution data >32.8 ka BP overlain by a 5-point unweighted smooth, black). Dashed line indicates modern subSST at 200 m water depth for Tobago Basin (Locarnini et al., 2018). **E)** $\delta^{18}O_{sw-ivf}$ (‰; high-resolution data >32.8 ka BP overlain by a 5-point unweighted smooth, black) approximating subsurface salinity. Dashed line indicates modern $\delta^{18}O_{sw}$ (‰ SMOW) at ~200 m (c.f. Jentzen et al., 2018a). **F)** Record of relative sea level change (Grant et al., 2012; gray; overlain by a 7-point unweighted smooth, black) used for the calculation of $\delta^{18}O_{sw-ivf}$. The conversion of [m] in [% SMOW] was accomplished using the Waelbroeck et al. (2002) relationship: RSL (‰ SMOW) = 0.00016-0.0085 * RSL (m). Brownish shadings mark Greenland Interstadials (GI) (Dansgaard et al., 1993; GS = Greenland Stadial). Triangles mark AMS^{14}C ages (black) and tuning tie lines (white) (c.f. Fig. 2). Error bars = standard deviation (2σ).

4.2 Subsurface Tobago Basin - development on millennial timescales

Between ~37 ka BP and ~32.8 ka BP, the $subSST_{Mg/Ca}$ in Tobago Basin core 235 are on average relatively cool (~14°C), with an overall large-amplitude and centennial-scale $subSST_{Mg/Ca}$ variability of up to 6°C (Fig. 4B). This is clearly cooler-by-2 to 4°C than during the subsequent time period, in particular during HS3 (~31 ka BP; Wary et al., 2015), HS2, and HS1, but rather close to late Holocene subSST conditions at ~200 m water depth (c.f. Figs. 5B, 5; Reißig et al., 2019). The $subSST_{Mg/Ca}$-record exhibiting a pronounced millennial-scale variability does not follow the stadial-interstadial (D/O) variability typical for the northern glacial climate variability. It is rather characterized by high-amplitude variations, and $subSST_{Mg/Ca}$-maxima occur during stadials and during transitional periods (Fig. 4B). The B-Tukey frequency spectrum (AnalySeries 2.0; Paillard et al., 1996) of the 5 point-smoothed $subSST_{Mg/Ca}$ record >32.8 ka BP indicates a dominant ~740 year-periodicity (Fig. 4B; c.f. discussion in Appendix Text A.1; Fig. A.6), which is half the D/O cycles of 1.470 years (Rahmstorf, 2003). We have no conclusive explanation, but the underlying periodicity in $subSST_{Mg/Ca}$ corroborates the validity of our core chronology, and suggests a regular pacing of the tropical West Atlantic ocean system. The average $subSST_{Mg/Ca}$ trend over the time period discussed tends to increase by ~1.5°C. The highly variable $\delta^{18}O_{sw-ivf}$ record is broadly related to $subSST_{Mg/Ca}$, with commonly fresher/cooler and more saline/warmer time periods (Fig. 4F).

In contrast to the late HS1 and YD subsurface conditions, which were interpreted in terms of efficient heat and salt accumulation in the STG and the related spread of warm and saline subsurface SMW towards our core location (Fig. 5 B, D; Reißig et al., 2019), the subsurface conditions between 37 ka BP and ~32.8 ka BP remained significantly cooler and fresher (Fig. 5B, D; Fig. 6).

We hence argue that the STG remained at a northerly position and that our core location was not affected by SMW, likely due to the overall low SMW formation rates at times of a more sluggish but varying AMOC (Henry et al., 2016; Lippold et al., 2019). We rather rate the centennial-scale cyclic variability in $subSST_{Mg/Ca}$ and similarly in $\delta^{18}O_{sw-ivf}$ in terms of the presence/non-presence of the NBC and subtle contributions from the NEC at the core location, driven by a recurrent intensification and relaxation of the trade wind regime. This is in line with fluctuations of dinocyst associations in core M35003-4 (c.f. Fig. 1) indicating that the Tobago Basin sea surface was influenced by mainly mesotrophic waters deriving from the South Equatorial Current (SEC) but temporally and increasingly in time by oligotrophic NEC (Vink et al., 2001; Fig. 4E).

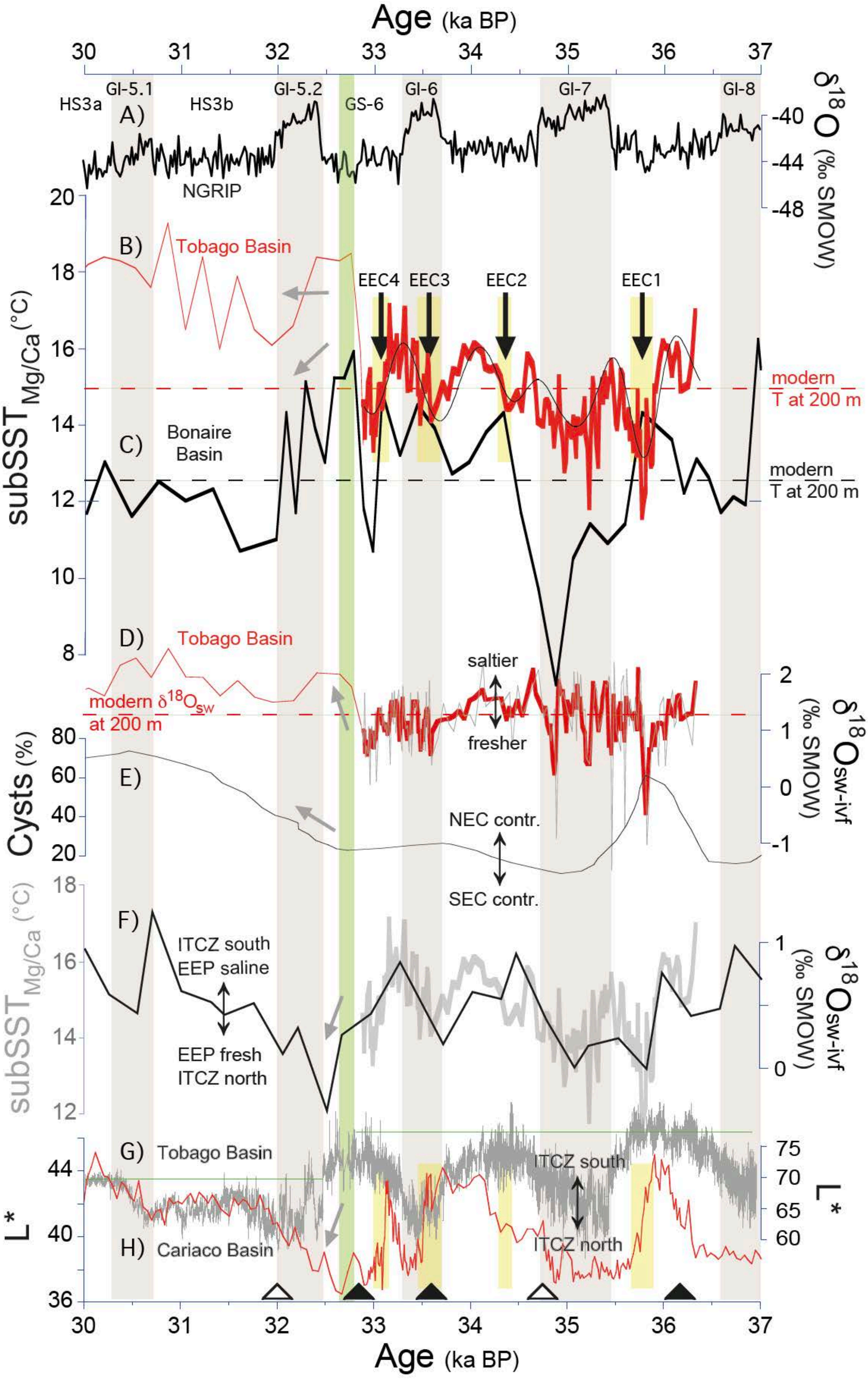
Age (ka BP)
30
31
32
33
34
35
36
37
HS3a
GI-5.1
HS3b
GI-5.2
GS-6
GI-6
GI-7
GI-8
A)
NGRIP
δ18O (‰ SMOW)
-40
-44
-48
B)
Tobago Basin
EEC4
EEC3
EEC2
EEC1
modern
T at 200 m
subSST Mg/Ca (°C)
20
18
16
14
12
10
8
C)
Bonaire
Basin
modern
T at 200 m
D)
Tobago Basin
modern δ18Osw
at 200 m
saltier
fresher
δ18Osw-ivf (‰ SMOW)
2
1
0
-1
Cysts (%)
80
60
40
20
E)
NEC contr.
SEC contr.
subSST Mg/Ca (°C)
18
16
14
12
F)
ITCZ south
EEP saline
EEP fresh
ITCZ north
δ18Osw-ivf (‰ SMOW)
1
0
G)
Tobago Basin
ITCZ south
ITCZ north
H)
Cariaco Basin
L*
44
40
36
75
70
65
60
Age (ka BP)

395

Fig. 4. Subsurface temperature and $\delta^{18}O_{sw-ivf}$ (salinity) development in Tobago Basin core M78/1-235-1 from 37–30 ka BP. Red curves = this study; black and gray curves = reference records. **A)** Greenland ice core $\delta^{18}O$ record as reference for the northern hemisphere climate signal (NGRIP Dating Group, 2006). **B)** $subSST_{Mg/Ca}$ record from Tobago Basin (this study; record >32.8 ka BP is 5-point unweighted smooth; c.f. Fig. 3); the overlying sinus curve depicts the 740-year filter output of the 5-point smoothed $subSST_{Mg/Ca}$ record >32.8 ka BP. **C)** $subSST_{Mg/Ca}$ record from Bonaire Basin (Parker et al., 2015) on a revised age model (black; c.f. Appendix Fig. A.7). Hatched lines in B) and C) indicate modern subSST at 200 m water depth for the Tobago and Bonaire basins (Locarnini et al., 2018). Black arrows and yellow shadings depict Tobago Basin subsurface cooling events synchronous to subsurface warming events in Bonaire Basin (Parker et al., 2015), termed events of equalized conditions (EEC1-4). **D)** Relative subsurface salinity changes approximated from *G. truncatulinoides* $\delta^{18}O_{sw-ivf}$ (this study; high-resolution data >32.8 ka BP are overlain by a 5-point unweighted smooth). Hatched line indicates modern $\delta^{18}O_{sw}$ (‰ SMOW) at ~200 m (c.f. Jentzen et al., 2018a). **E)** Relative abundances of calcareous dinocysts (*Calciodinellum albatrosianum*) in Tobago Basin (Vink et al., 2001; core M35003-4; c.f. Fig. 1) reflecting relative NEC vs. SEC (= South Equatorial Current) contributions. **F)** Equatorial East Pacific (EEP) salinity record of Leduc et al. (2007) reflecting moisture transport across Central America in line to ITCZ migrations (black; saline EEP = ITCZ at south). The record >32.8 ka BP is underlain by the smoothed Tobago Basin $subSST_{Mg/Ca}$ record (c.f. B); gray), implying considerable consonance. **G)** Core 235 sediment reflectance L*. **H)** Sediment reflectance L* data from Cariaco Basin (Deplazes et al., 2013). Green horizontal lines denote a general sedimentological change at ~32.8 ka BP, in line with changes in the tropical West Atlantic (B-E) and the equatorial East Pacific (F). Gray shadings mark Greenland Interstadials (GI). Heinrich Stadial HS 3 is indicated (HS 3a and 3b). Green shading marks prominent transition at ~32.8 ka BP. Gray arrows mark prominent trend changes in proxy parameters. Triangles indicate $AMS^{14}C$ ages (black) and tuning tie lines (white) (c.f. Fig. 2).

The interannual to multidecadal variations of the tropical atmospheric water cycle and the associated cross-isthmus moisture transport (Leduc et al., 2007) appear important for the subsurface temperature and salinity changes before ~32.8 ka BP. Leduc et al. (2007) stated that a southerly position of the ITCZ caused the orogenic blocking of westward directed atmospheric moisture transport by the Andes, leading to higher saline sea surface conditions in the Equatorial East Pacific (EEP). At the same time, the returned freshwater supply into the tropical West Atlantic *via* the Amazon drainage system should have lowered salinity in the NBC, the GC and the CC entering the Caribbean (Leduc et al., 2007). The Tobago Basin subsurface salinity record is not conclusive in this respect, as *G. truncatulinoides* as proxy carrier likely dwells too deep to trace the shallow freshwater contribution. However, the ample correlation between the cyclic $subSST_{Mg/Ca}$ variations in Tobago Basin and the sea surface salinity variations in the EEP (Fig. 4F) suggests a common driving force behind. Warm and commonly more saline subsurface conditions pointing to expanded NEC at the expense of cool and fresh NBC during times of a southern ITCZ correlate to saline EEP conditions, which occur when the ITCZ is also south. Similarly, the millennial-scale sea surface salinity variations in Florida Strait were interpreted in terms of variations in the evaporation/precipitation balance in the tropical Atlantic in response to the strength and north-south shifts of the ITCZ across D/O stadial/interstadial changes (Them et al., 2015). We conclude that during this time period of intermediate glacial conditions, Tobago Basin was not yet affected by SMW as it was during HS1 and the YD (c.f. Reißig et al., 2019), most likely due to the fact that the STG temperature and salinity conditions were not optimal allowing for sufficient SMW formation and its southward dispersal (c.f. Fig. 5B, C).

4.3 Events of equalized conditions in the Tobago and Bonaire basins

The cyclic development in Tobago Basin $subSST_{Mg/Ca}$ between 37-32.8 ka BP is different to the rather low-resolved $subSST_{Mg/Ca}$ variability in the close-by Bonaire Basin (Parker et al., 2015), however, both records display a systematic relationship (Fig. 4B, C). Short-term deflections to cool (~3-4°C cooler than modern; down to ~10°C) and fresh subsurface conditions in Tobago Basin appear synchronous to the pulse-like subsurface warming events by up to ~4°C in Bonaire basin (Parker et al., 2015; similarly reconstructed from $Mg/Ca_{\mathit{G.truncatulinoides}}$) leading to equal (within $\pm$1°C) and/or converging conditions in both regions (termed Events of Equalized Conditions EEC4 to 1 in Fig. 4B and 6) during Greenland stadials as well as interstadials (GS-8 at ~35.7 ka BP; GS-7 at ~34.4 ka BP; GS-6 at ~33.1 ka BP and GI-6 at ~33.5 ka BP). Due to the carefully established age models of both records (c.f. Appendix Fig. A.7), we consider these temporal relationships between basins robust. Following the ideas of Schmidt et. (2012), Parker et al. (2015) initially explained the Bonaire subsurface warming events by the strengthened influx of SMW into Bonaire Basin at times of an extended STG, a reduced WBC (namely NBC), and a weakened AMOC.

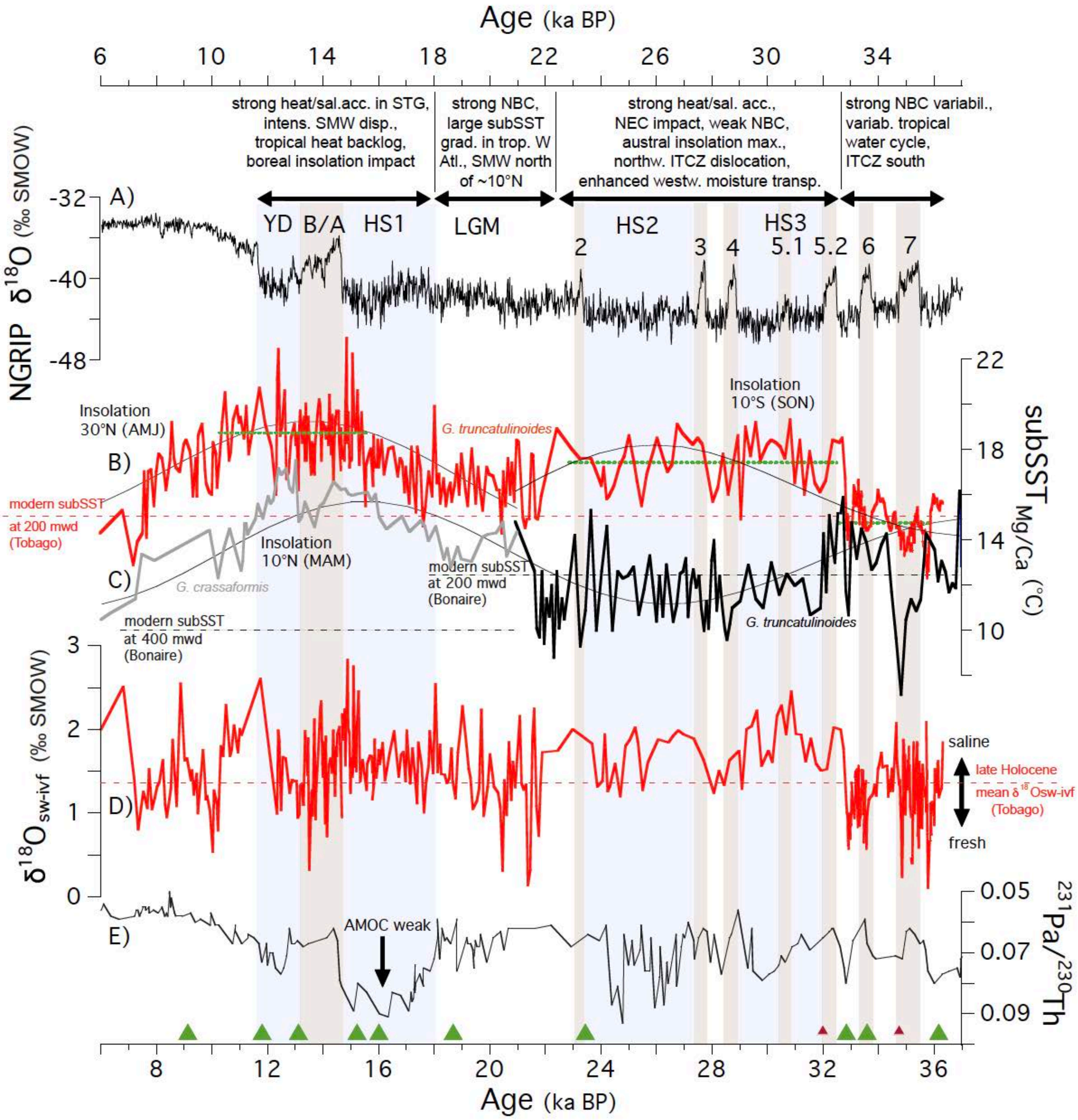

Fig. 5. Subsurface water dynamics in the tropical West Atlantic from 37-6 ka BP. Red curves = Tobago Basin core 235 (this study; Reißig et al., 2019; data >32.8 ka BP are 5-point smoothed); black and gray curves = reference records. **A)** Greenland ice core δ^{18}O record as reference for the northern hemisphere climate signal (NGRIP Dating Group, 2006).

B) $subSST_{Mg/Ca}$ record from core 235 (red) (this study; $subSST_{Mg/Ca}$ <30 ka based on raw $Mg/Ca_{G.truncatulinoides}$ of Reißig et al., 2019). Green dotted lines denote $subSST_{Mg/Ca}$ averages: 14.8°C for 36.3-32.8 ka BP; 17.5°C for 32.7-23.3 ka BP; 18.7°C for 15.4-10.5 ka BP. The $subSST_{Mg/Ca}$ follow the 10°S austral insolation (Sept. to Nov.; SON) until ~21.8 ka BP; afterwards the 30°N boreal insolation (Apr. to June; AMJ). **C)** $subSST_{Mg/Ca}$ records from Bonaire Basin (black: based on $Mg/Ca_{G.truncatulinoides}$; Parker et al., 2015, on a revised age model, see Appendix; gray: based on $Mg/Ca_{G.crassaformis}$; Schmidt et al., 2012). The Bonaire record follows the 10°N boreal insolation (Mar. to May; MAM) over the entire time period. **D)** $\delta^{18}O_{sw-ivf}$ approximating relative subsurface salinity changes (this study; Reißig et al., 2019). **E)** $^{231}Pa/^{230}Th$ record from Bermuda Rise (Henry et al., 2016; Lippold et al., 2019) used as indicator of AMOC strength. Dashed lines mark modern subsurface water temperatures, differentiated into regions and habitat depths in B) and C), and the modern East Caribbean $\delta^{18}O_{sw-ivf}$-value at subsurface (200 m; Jentzen et al., 2018a) in D). Gray shadings mark Greenland Interstadials (GI) and the B/A; blue shadings mark Heinrich Stadials HS3, HS2, HS1, and the YD. Large green triangles mark AMS^{14}C datings; small brown triangles mark further tuning tie lines used for stratigraphical purposes (c.f. Fig. 2). Top panel accentuates the paleoceanographic/paleoclimatic development.

Alternatively to Parker et al. (2015), we suggest a different mechanism to explain both the short-term subsurface warming pulses in Bonaire Basin and the equalization of $subSST_{Mg/Ca}$ conditions. We have to keep in mind that first the subsurface warming episodes in Bonaire Basin (Parker e al., 2015) remained significantly cooler by ~2-3°C than the deglacial subsurface warming events (HS1 and YD) described in the same core 107 (Schmidt et al., 2012; 16-17°C based on $Mg/Ca_{G.crassaformis}$ implying that $subSST_{Mg/Ca}$-estimates from the shallower-living *G. truncatulinoides* would have been even warmer!) (see further discussion below). Second, the $subSST_{Mg/Ca}$ in Tobago Basin remained cooler by several degrees than during the deglacial periods of AMOC weakening (HS1 and YD), for which a southward extended STG and enhanced SMW formation were proposed (Reißig et al., 2019) (c.f. Fig. 5B, C). Third, the EECs appear synchronous to rapid transitions from high (light) to low (dark) L* values during Greenland stadials GS-8, GS-6 and interstadial GI-6 in core 235 (Fig. 4G; GS-7 is exceptional in this respect). Following Hoffmann et al. (2014), we rate the prominent L*-changes with low L* pointing to high terrigenous riverine input as regional expression of rapid ITCZ migrations across the study area from south to north corresponding to the short-term variability of the tropical climate system. Differences between the Tobago and the well-known Cariaco L*-records (Deplazes et al., 2013; core MD03-2621, c.f. Fig. 1A) might have arisen from seasonal bias being different in both areas. Local variations and changes in productivity due to regional upwelling or differences in river run-off and nutrient inputs, might have added to the differences in the L*-records (Fig. 4G, H).

We hypothesize that during these short EECs accompanied by northward ITCZ movements (c.f. Fig. 4F, G, H), the intensified northward flowing NBC caused subsurface cooling and relative freshening in the overall warm and saline Tobago Basin on the one hand. On the other hand, the strong NBC is still warm enough to cause relative subsurface warming when invading into the overall cool Bonaire Basin (Fig. 4B, C). We emphasize that Bonaire Basin is a region of (seasonal) coastal upwelling (Haug et al., 2001), and subsurface conditions during glacial times were commonly cooler by >2°C than in Tobago Basin (Fig. 4B, C). This fundamental difference in subSST conditions between both basins is also valid today, due to the different geographical and oceanographic settings (c.f. Fig. 1). Overall, the centennial-scale EECs point to a highly dynamic and variable NBC, which is closely related to a rapidly changing and unsteady upper ocean–atmosphere system in the tropical West Atlantic.

4.4 Rapid subsurface re-organization at ~32.8 ka BP persisting until 21.8 ka

A major and rapid re-organization of the subsurface Caribbean and tropical West Atlantic occurred around the transition from stadial GS-6 to interstadial GI-5.2, leading to regionally clearly differentiated subsurface conditions until ~21 ka BP (Figs. 4B,C, 5B,C). After ~32.8 ka BP, the $subSST_{Mg/Ca}$ in Tobago Basin increase within ~100 years by up to ~5°C and remain on average higher-by-~3°C than before (Fig. 4B). This glacial $subSST_{Mg/Ca}$ level is clearly higher by ~2-3°C than the modern $subSST_{200m}$ of ~15.5°C at the site location. The prominent subsurface warming is accompanied by a change to more saline conditions (subsurface $\delta^{18}O_{sw-ivf}$ >1.5 ‰ and even up to 2.5 ‰) with maxima during HS3 (Fig. 4D), becoming equal to conditions described further to the north in the central Caribbean (Beata Ridge core SO164-03-4; Reißig et al., 2019). Similarly, Hüls and Zahn (2000) documented a subsurface temperature increase equal in amplitude at ~100 m water depth in Tobago Basin at ~32.5 ka BP, deduced from foraminiferal Modern Analogue Technique estimates, but did not further comment on this prominent change.

The prominent subsurface warming in Tobago Basin is paralleled by same-amplitude subsurface cooling in Bonaire Basin with the end of GS-6 and during the run of GI-5.2, basically terminating the previous (>32.8 ka BP) cyclic subsurface temperature development in Tobago Basin and the temporally converging $subSST_{Mg/Ca}$ in both basins (Fig. 4B, C). The $subSST_{Mg/Ca}$ record from Bonaire Basin (Parker et al., 2015) continuously cooled by ~3-4°C, thereby becoming even lower than the modern Bonaire Basin subSST of ~12.5°C (Fig. 4C). As the $subSST_{Mg/Ca}$ in Tobago Basin remained rather high (on average 17°C), the $subSST_{Mg/Ca}$ gradient between both basins prominently increased to on average ~5.5°C, which broadly remained until ~21.8 ka BP (Figs. 4, 5B, C). Other processes than the previously noted ITCZ-related NBC dynamics apparently took over and began to create clearly separated oceanographic conditions in both regions.

The timing of this prominent subsurface change across GS-6 and GI-5.2 is supported by the Cariaco Basin sediment reflectance (L*) record (Deplazes et al., 2013), which shows a characteristic shift in the L*-level from high (max. ~77) to lower values (max. ~70), and a clear decline in amplitude (Fig. 4F). This prominent shift in the L*-level towards overall darker sediment colors is interpreted as a slight but persistent northward dislocation of the still southern ITCZ, which likely caused higher terrigenous matter supply and lowered oxygen conditions in Cariaco Basin than before. In core 235, the shift in L* across GS-6 and GI-5.2 is less prominent and highly variable (Fig. 4D), implying changing fluvial supply of terrigenous matter, likely due to the fact that the ITCZ varied across the catchment areas of the South American river systems (Orinoco, also Amazon), which deliver the terrigenous freight towards our coring location 235.

After the significant and rapid change across GS-6 and during the run of GI-5.2, the Tobago Basin subsurface conditions remained rather warm although variable until ~21.8 ka BP (MIS 2) (Fig. 5B). The warmer-by-~3°C and more saline subsurface conditions (>1 ‰ $\delta^{18}O_{sw-ivf}$) were likely due to the increasing influence of warm and saline subsurface water from the NEC. Indeed, the dinocyst assemblage change in Tobago Basin at ~32.5 ka BP points to the amplified and persisting presence of oligotrophic NEC waters (Vink et al. 2001) (Fig. 4E; c.f. Fig. 1). The synchronous decrease of *Neogloboquadrina dutertrei* implies a considerable change to higher salinities (Zahn and Stüber, 2002). The temporal presence of warm and saline NEC waters was likely associated with an equatorward compression of climatic belts leading to more zonal winds in both hemispheres, and an accelerated atmospheric circulation. The corresponding strong trade winds might well have intensified the NBC retroflection and countercurrent preventing cool and fresh NBC waters to pass into the Caribbean *via* the GC and the CC (c.f. Fig. 1C, E).

We argue that during 32.6-21.8 ka BP the ITCZ-related displacements of the (sub)tropical wind system best explain NEC/NBC interactions and related oceanographic processes in Tobago Basin, as well as ocean heat transport *via* the NEC-coined Caribbean Current into the Gulf of Mexico and Florida Straits. Following the argumentation of Leduc et al. (2007), the enhanced build-up of saline conditions in the subtropical Atlantic (Fig. 4D) would have been promoted by enhanced westward atmospheric moisture transport across Central America in line with an ITCZ position, which moved further to the north after ~32.8 ka BP. Model results of Zhang et al. (2017 and references therein) point out that increasing salinity in the subtropical North Atlantic due to an enhanced westward moisture transport across

Central America in response to a gradual atmospheric CO_2 change (Ahn and Brook, 2014) is a prerequisite for the onset of Heinrich events, as it modulates the freshwater budget of the North Atlantic and hence deep-water formation. This would be in line with the observation that the divergent subSST$_{Mg/Ca}$ pattern between Tobago and Bonaire basins and the rapid development to warmer and saline subsurface conditions in Tobago Basin evolved during GI-5.2, a couple of hundred years before the onset of HS3 (Fig. 5B, C, D).

The rapidly declining influence of (relatively warm) NBC waters entering the Caribbean Sea *via* the Lesser Antilles passages since ~32.8 ka BP might have been mastermind to the observed subsurface cooling by ~3-4°C in Bonaire Basin (coming close to modern conditions, with considerable subSST$_{Mg/Ca}$-amplitude variations in particular during HS2) (Fig. 5C). The gradual strengthening of the trade winds during times of climatic aggravation (reflected in the lowering of the global sea level since then; Grant et al., 2012; Fig. 3F) likely fostered coastal upwelling (Peterson et al., 2000) and a cool upper water column in Bonaire Basin (Parker et al., 2015).

The subsurface conditions described came rapidly to an end at ~21.8 ka BP. Significant subsurface cooling and freshening within a few hundreds of years occurred in Tobago Basin (Fig. 5B, D), while remaining fresher than in the central Caribbean (Beata Ridge core SO164-03-4; Reißig et al., 2019; Fig. 1). In contrast, the Bonaire Basin subSST$_{Mg/Ca}$ (inferred from Mg/Ca$_{\mathit{G.truncatulinoides}}$; Parker et al., 2015) rapidly increase, becoming similar to the subsequent Mg/Ca$_{\mathit{G.crassaformis}}$-derived subSST$_{Mg/Ca}$ (Schmidt et al., 2012) (Fig. 5C). Considering that the latter reflects deeper conditions than the Mg/Ca$_{\mathit{G.truncatulinoides}}$-derived subSST$_{Mg/Ca}$ implies that after ~21.8 ka BP Bonaire Basin must have been even warmer at 200 m water depth coming close to the cool Tobago Basin subsurface conditions. The subSST$_{Mg/Ca}$ gradient between both basins hence rapidly vanished at ~21.8 ka BP (Fig. 5B, C).

In view of the cool and fresh subsurface conditions in Tobago Basin during ~21.8-18 ka BP being rather close/similar to those conditions existing before ~32.8 ka BP (see above, Fig. 5B, D), we assume that at full glacial times the impact of the NBC increased again. For full glacial times, Reißig et al. (2019) described distinctive gradients in $subSST_{Mg/Ca}$ and subsurface $\delta^{18}O_{sw-ivf}$ established across the tropical West Atlantic, with a deep thermocline and warm and saline subsurface conditions in the central Caribbean (Beata Ridge), cool and fresh subsurface conditions in Tobago Basin further to the south, and equally cool (or even cooler) subsurface conditions in Bonaire Basin. If considerable quantities of subsurface SMW were formed through Ekman downwelling within the STG, then they might have affected the central Caribbean, but neither Tobago nor Bonaire basins. These remained under the influence of the relatively strong NBC, keeping the warm/salty waters of the STG north of ~10°N (c.f. Fig. 6).

4.5 Differential tropical West Atlantic functioning during cool periods

Figure 6 summarizes the temporally very different subsurface conditions in Tobago Basin during the cool climate periods of the last 37 kyrs, based on core 235 $subSST_{Mg/Ca}$ and subsurface $\delta^{18}O_{sw-ivf}$ data (this study; Reißig et al., 2019) in comparison to the modern conditions. Prior to ~32.8 ka and during the EECs, the subsurface conditions were mostly cooler (>2°C) and more saline than today. The $subSST_{Mg/Ca}$ during the LGM and during HS3 and HS2 were close to modern conditions, but conditions were more saline. Late HS1 and the YD appear very different, as they were significantly warmer (>3°C) and more saline than today and than during the previous cool time periods.

Model simulations from Zhu et al. (2014) and Chang et al. (2008) propose a mechanistic coupling between the tropical West Atlantic subsurface heat accumulation and AMOC weakening (c.f. Chapter 1). The question raises why the subsurface conditions differed between Tobago (this study) and Bonaire basins (Parker et al., 2015) during HS3 and HS2, but became rather similar during HS1 (Schmidt et al., 2012), although all Heinrich stadials similarly were characterized by temporal AMOC weakening (e.g. Lippold et al., 2009) (Fig. 5B, C, E). We hypothesize that in addition to AMOC weakening, further internal and external processes exert significant control on the subsurface development of the tropical West Atlantic.

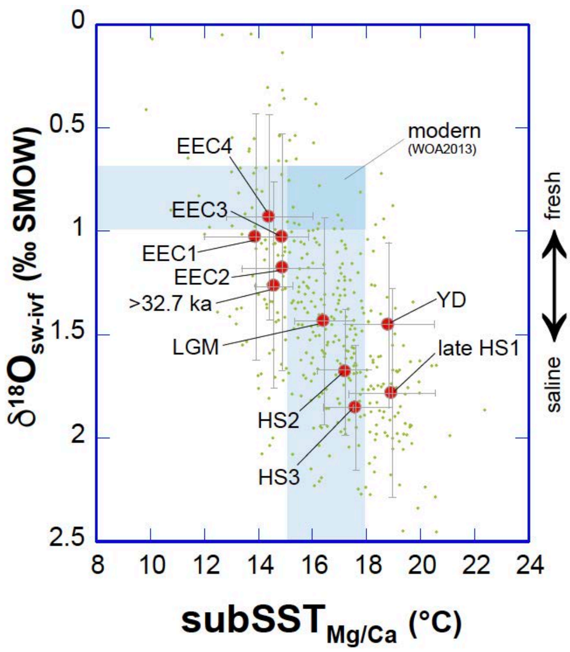

Fig. 6. Subsurface $\delta^{18}O_{sw\text{-}ivf}$ and subSST$_{Mg/Ca}$ data of core 235 (green dots; this study, Reißig et al., 2019), averaged for distinct time periods (large red dots), in comparison to modern conditions (bluish rectangular). Modern subsurface (~200 m water depth) temperatures were taken from Locarnini et al. (2013) at the core location. Modern subsurface $\delta^{18}O_{sw}$ was calculated from modern subsurface salinities (Locarnini et al., 2013) using the $\delta^{18}O_{sw}$ vs. salinity regression equations from Schmidt et al. (1999) and Jentzen et al. (2018a). These calculations are consistent to measured eastern Caribbean $\delta^{18}O_{sw}$ values (Jentzen et al., 2018a). Past time periods: YD = Younger Dryas, late HS1 = Heinrich Stadial 1, LGM = Last Glacial Maximum, HS2 = Heinrich Stadial 2, HS3 = Heinrich Stadial 3, >32.8 = average from 32.8-36.1 ka BP, EEC1-4 = events of equalized conditions. Note that EECs are cooler than modern conditions; deglacial periods of AMOC perturbations (YD, HS1) are clearly warmer and more saline than modern conditions. Error bars included.

The Bonaire Basin subSST$_{Mg/Ca}$ record broadly follows the local boreal spring insolation (March to May) at 10°N since 32.5 ka BP (Fig. 5C). In particular during HS3 and HS2, the subSST$_{Mg/Ca}$ remained cool and close to modern conditions, due to intense (spring) upwelling during times of climate aggravation, low sea level, and low 10°N insolation. After ~21.8 ka BP, however, the subSST$_{Mg/Ca}$ increase due to the strengthened impact of SMW (Schmidt et al., 2012), thereby closely following the northern hemisphere insolation to which the STG dynamics is coupled.

The Tobago Basin subSST$_{Mg/Ca}$ record, instead, follows the 10°S austral early summer insolation (September to November) from ~32.5 ka BP to ~21.8 ka BP, apparently capturing the southern hemisphere climate signal. This appears reasonable as the NBC being responsible for the subSST$_{Mg/Ca}$ development is branching off from the SEC at ~10°S off the Brazilian continental margin (e.g. Johns et al., 2002). In particular during HS3 and HS2 the subSST$_{Mg/Ca}$ gradient towards the cool Bonaire Basin raises up by >5°C, when 10°N and 10°S insolation records are most opposite to each other (Fig. 5B, C).

With the beginning deglaciation, the Tobago Basin subSST$_{Mg/Ca}$ record no longer follows the 10°S austral early summer insolation, but the 30°N boreal early summer (April/May/June) insolation, suggesting that the impact of the southern hemisphere was gradually replaced by climate processes of the northern hemisphere. The subSST$_{Mg/Ca}$ culminate in extremely high values during the deglaciation (~18.7°C, averaged for 15.5-10.5 ka BP; c.f. Reißig et al., 2019), and become rather similar to the extremely warm subSST$_{Mg/Ca}$ in Bonaire Basin (Schmidt et al., 2012) (Fig. 5B, C). This critical heat and salinity accumulation causing a deep thermocline and low lateral gradients at subsurface across the tropical West Atlantic demands for the intensified formation of warm and high-saline SMW (c.f. Reißig et al., 2019; Schmidt et al., 2012). Promoted by high northern hemisphere insolation in the STG area (~30°N) favoring evaporation, the southern ITCZ (Arbuszewski et al., 2013; Broccoli et al., 2006; Chiang and Bitz, 2005; Vink et al., 2001), the associated shifts of hydrographic and atmospheric frontal systems (Barker et al., 2009), higher wind stress (Vellinga and Wu, 2004), and the weakened or even reversed NBC (Bahr et al., 2018; Zhang et al., 2015), SMW increasingly formed due to strengthened Ekman-downwelling in the STG area, and entered the subsurface tropical West Atlantic. This was not achieved before late HS1, when AMOC weakening and according tropical heat backlog on the one hand (e.g. Henry et al., 2016) and maximum Northern Hemisphere insolation during times of rising sea level and climate amelioration on the other hand acted together. Notably, during the YD the tropical West Atlantic subsurface conditions were rather similar to those of HS1 (Fig. 5B), although $^{231}Pa/^{230}Th$-based reconstructions imply that the AMOC was operating more actively (Ng et al., 2015; McManus et al., 2004), and tropical ocean heat should have increasingly been withdrawn towards the North Atlantic. This discrepancy may point to a muted response of the STG to AMOC perturbations.

5. Conclusions

The centennial to millennial-resolving subsurface proxy records from Tobago Basin core 235 spanning the D/O time period from ~37-30 ka BP of intermediate glacial conditions reveal cool and fresh subsurface conditions. The subtle millennial-scale variations were interpreted in terms of the presence/non-presence of the NBC, which acted in concert to a recurrent intensification and relaxation of the trade wind regime and subtle migrations of the ITCZ at times when the AMOC-variability was rather muted. The ITCZ remained at an overall southern position, leading to the orogenic blocking of westward directed moisture transport by the Andes, to an enhanced freshwater supply into the tropical West Atlantic *via* the Amazon drainage, and to lowered salinity in the NBC flowing northward towards the Caribbean.

The cyclic $subSST_{Mg/Ca}$ development in Tobago Basin and the temporally equalized subsurface conditions in the Tobago and Bonaire basins during Greenland stadials as well as interstadials (GS-8 at ~35.7 ka BP; GS-7 at ~34.4 ka BP; GS-6 at ~33.1 ka BP and GI-6 at ~33.5 ka BP) are explained by a periodically changing NBC. The strengthened presence of NBC caused subsurface cooling and freshening in the overall warm and saline Tobago Basin, while synchronously causing relative subsurface warming in the overall cool Bonaire Basin.

A major re-organization of the subsurface Caribbean and tropical West Atlantic occurred within ~100 years at ~32.8 ka BP, related to both a weakened or even retroflected NBC and the gradually rising impact of NEC. Supported by the increasing austral spring insolation, subsurface waters in Tobago Basin warmed considerably. This change was associated with the enhanced build-up of saline conditions that were promoted by enhanced westward moisture transport across Central America in line with an ITCZ position, which moved clearly further to the north after ~32.8 ka BP. In comparison to already published proxy datasets from the same Tobago Basin core 235 we conclude that it is not before the late HS1 that formation of SMW in the STG area and its southward subsurface dispersal intensified, reaching far south into both the Bonaire and Tobago basins.

Acknowledgements

We thank the German Science Foundation (DFG), which in the framework of the 'Cluster of Excellence – The Future Ocean' (Univ. Kiel) provided funding to generate in parts the data presented here. We thank former Ph.D. students S. Reißig and D. Poggemann, as well as lab technicians N. Gehre and S. Fessler for great support. We are grateful to S. Szidat from the University of Bern, J. Hoffmann from Frankfurt University, and Beta Analytic Limited, UK, for AMS^{14}C measurements. We thank the captain, crew, and shipboard scientific crew of R/V METEOR for their support. R/V Meteor cruise M78 was funded by the DFG under project 194018713. We also acknowledge funding from the DFG through projects HO 5927/1-1 (to

AB) and LI 1815/4 (to JL). CK thanks for funding from ANID/Millennium Science Initiative/Millennium Nucleus Paleoclimate NCN17_079. We are thankful to the reviewers, whose comments considerably helped to improve the manuscript.

Data availability

Presented data (Nürnberg et al. (2020) are available online at the Data Publisher for Earth and Environmental Science, PANGEA (www.pangaea.de): https://doi.org/10.1594/PANGAEA.919497.

Appendix A.

Supporting information associated with this article can be found in the Appendix.

References

Ahn, J., Brook, E. (2014). Siple Dome ice reveals two modes of millennial CO_2 change during the last ice age. Nature Communication 5, 3723. https://doi.org/10.1038/ncomms4723.

Arbuszewski, J.A., deMenocal, P.B., Cléroux, C., Bradtmiller, L., Mix, A. (2013). Meridional shifts of the Atlantic intertropical convergence zone since the Last Glacial Maximum. Nature Geoscience 6 (11), 959–962.

Bahr, A., Nürnberg, D., Karas, C., Grützner, J. (2013). Millennial-scale versus long-term dynamics in the surface and subsurface of the western North Atlantic Subtropical Gyre during marine isotope stage 5. Global and Planetary Change 111, 77–87. https://doi.org/10.1016/j.gloplacha.2013.08.013.

Bahr, A., Hoffmann, J., Schönfeld, J., Schmidt, M.W., Nürnberg, D., Batenburg, S.J., Voigt, S. (2018). Low-latitude expressions of high-latitude forcing during Heinrich Stadial 1 and the Younger Dryas in northern South America. Global and Planetary Change 160, 1–9.

Barker, S., Diz, P. (2014). Timing of the descent into the last Ice Age determined by the bipolar seesaw. Paleoceanography 29 (6), 489–507.

Barker, S., Diz, P., Vautravers, M.J., Pike, J., Knorr, G., Hall, I.R., Broecker, W.S. (2009). Interhemispheric Atlantic seesaw response during the last deglaciation. Nature 457 (7233), 1097–1102.

Blanke, B. (2002). A Lagrangian numerical investigation of the origins and fates of the salinity maximum water in the Atlantic. Journal of Geophysical Research 107 (C10), 1038.

Blaauw, M., Christen, J.A. (2011). Flexible paleoclimate age-depth models using the autoregressive gamma process. Bayesian Analysis 6 (3), 457-474. doi:10.1214/11-BA618. https://projecteuclid.org/euclid.ba/1339616472.

Boyle, E.A., Keigwin, L.D. (1985/86). Comparison of Atlantic and Pacific paleochemical records for the last 215,000 years: changes in deep ocean circulation and chemical inventories. Earth Planetary Science Letters 76, 135-150.

Boyle, E.A., Rosenthal, Y. (1996). Chemical hydrography of the South Atlantic during the Last Glacial Maximum: Cd vs. $\delta^{13}C$. In: Wefer, G., Berger, W.H., Siedler, G., Webb, D. (eds.), The South Atlantic: Present and Past Circulation, Springer, Berlin, Heidelberg, 423-443.

Broccoli, A.J., Dahl, K.A., Stouffer, R.J. (2006). Response of the ITCZ to Northern Hemisphere cooling. Geophysical Research Letters 33 (1), L01702. https://doi.org/10.1029/2005GL024546.

Buckley, M.W., Marshall, J. (2016). Observations, inferences, and mechanisms of the Atlantic Meridional Overturning Circulation: A review. Reviews of Geophysics 54 (1), 5–63.

Caley, T., Roche, D.M. (2015). Modeling water isotopologues during the last glacial: Implications for quantitative paleosalinity reconstruction. Paleoceanography 30 (6), 739–750.

Calvo, E., Villanueva, J., Grimalt, J. O., Boelaert, A., Labeyrie, L. (2001). New insights into the glacial latitudinal temperature gradients in the North Atlantic. Results from UK′37 sea surface temperatures and terrigenous inputs. Earth and Planetary Science Letters 188 (3–4), 509–519. https://doi.org/10.1016/S0012-821X(01)00316-8.

Chang, P., Zhang, R., Hazeleger, W., Wen, C., Wan, X., Ji, L., Haarsma, R.J., Breugem, W.- P., Seidel, H. (2008). Oceanic link between abrupt changes in the North Atlantic Ocean and the African monsoon. Nature Geoscience 1 (7), 444–448.

Chiang, J.C.H., Bitz, C.M. (2005). Influence of high latitude ice cover on the marine Intertropical Convergence Zone. Climate Dynamics 25 (5), 477–496.

Cléroux, C., Cortijo, E., Anand, P., Labeyrie, L., Bassinot, F., Caillon, N., Duplessy, J.-C. (2008). Mg/Ca and Sr/Ca ratios in planktonic foraminifera: Proxies for upper water column temperature reconstruction. Paleoceanography 23, PA3214. https://doi.org/10.1029/2007PA001505.

Dansgaard, W., Johnsen, S.J., Clausen, H.B., Dahl-Jensen, D., Gundestrup, N.S., Hammer, C.U., Hvidberg, C.S., Steffensen, J.P., Sveinbjörnsdottir, A.E., Jouzel, J., Bond, G. (1993). Evidence for general instability of past climate from a 250-kyr ice-core record. Nature 364 (6434), 218–220.

Deplazes, G., Lückge, A., Peterson, L.C., Timmermann, A., Hamann, Y., Hughen, K.A., Röhl, U., Laj, C., Cane, M.A., Sigman, D.M., Haug, G.H. (2013). Links between tropical rainfall and North Atlantic climate during the last glacial period. Nature Geoscience 6 (3), 213– 217.

Drijfhout, S.S., Hazeleger, W. (2006). Changes in MOC and gyre-induced Atlantic Ocean heat transport. Geophysical Research Letters 33 (7), 164.

EPICA Commuity Member (2006). One-to-one coupling of glacial climate variability in Greenland and Antarctica. Nature 444 (7116), 195–198.

Fratantoni, D.M., Johns, W.E., Townsend, T.L., Hurlburt, H.E. (2000). Low-Latitude Circulation and Mass Transport Pathways in a Model of the Tropical Atlantic Ocean. Journal of Physical Oceanography 30 (8), 1944–1966.

Grant, K.M., Rohling, E.J., Bar-Matthews, M., Ayalon, A., Medina-Elizalde, M., Ramsey, C.B., Satow, C., Roberts, A.P. (2012). Rapid coupling between ice volume and polar temperature over the past 150,000 years. Nature 491 (7426), 744–747.

Greaves, M., Caillon, N., Rebaubier, H., Bartoli, G., Bohaty, S., Cacho, I., Clarke, L., Cooper, M., Daunt, C., Delaney, M., deMenocal, P., Dutton, A., Eggins, S., Elderfield, H., Garbe- Schoenberg, D., Goddard, E., Green, D., Groeneveld, J., Hastings, D., Hathorne, E., Kimoto, K., Klinkhammer, G., Labeyrie, L., Lea, D.W., Marchitto, T., Martínez-Botí, M.A., Mortyn, P.G., Ni, Y., Nürnberg, D., Paradis, G., Pena, L., Quinn, T., Rosenthal, Y., Russell, A., Sagawa, T., Sosdian, S., Stott, L., Tachikawa, K., Tappa, E., Thunell, R., Wilson, P.A. (2008). Interlaboratory comparison study of calibration standards for foraminiferal Mg/Ca thermometry. Geochemistry, Geophysics, Geosystems 9 (8), https://doi.org/10.1029/2008GC001974.

Häkkinen, S., Rhines, P.B., Worthen, D.L. (2011). Warm and saline events embedded in the meridional circulation of the northern North Atlantic. Journal of Geophysical Research 116 (C3), 1.

Hátún, H., Sandø, A.B., Drange, H., Hansen, B., Valdimarsson, H. (2005). Influence of the Atlantic subpolar gyre on the thermohaline circulation. Science (New York, N.Y.) 309 (5742), 1841–1844.

Haug, G.H., Hughen, K.A., Sigman, D.M., Peterson, L.S., Röhl, U. (2001). Southward migration of the Intertropical Convergence Zone through the Holocene. Science 293 (5533), 1304-1308, https://doi.org/10.1126/science.1059725.

Hellweger, F.L., Gordon, A.L. (2002). Tracing Amazon River water into the Caribbean Sea. Journal of Marine

Research 60 (4), 537–549.

Henry, L.G., McManus, J.F., Curry, W.B., Roberts, N.L., Piotrowski, A.M., Keigwin, L.D. (2016). North Atlantic ocean circulation and abrupt climate change during the last glaciation. Science, 353 (6298), 470-474. doi: 10.1126/science.aaf5529.

Hernández-Guerra, A., Joyce, T.M. (2000). Water masses and circulation in the surface layers of the Caribbean at 66°W. Geophysical Research Letters 27 (21), 3497–3500.

Hoffmann, J., Bahr, A., Voigt, S., Schönfeld, J., Nürnberg, D., Rethemeyer, J. (2014). Disentangling abrupt deglacial hydrological changes in northern South America: Insolation versus oceanic forcing. Geology 42 (7), 579–582.

Hu, C., Montgomery, E.T., Schmitt, R.W., Muller-Karger, F.E. (2004). The dispersal of the Amazon and Orinoco River water in the tropical Atlantic and Caribbean Sea: Observation from space and S-PALACE floats. Deep Sea Research Part II: Topical Studies in Oceanography 51 (10-11), 1151–1171.

Hüls, M., Zahn, R. (2000). Millennial scale sea surface temperature variability in the western tropical North Atlantic from planktonic foraminiferal census counts. Paleoceanography, 15 (6), 659–678. https://doi.org/10.1029/1999PA000462.

Jentzen, A., Nürnberg, D., Hathorne, E. C., Schönfeld, J. (2018a). Mg / Ca and $\delta^{18}O$ in living planktic foraminifers from the Caribbean, Gulf of Mexico and Florida Straits. Biogeosciences 15 (23), 7077-7095. doi:10.5194/bg-15-7077-2018.

Jentzen, A., Schönfeld, J., Schiebel, R. (2018b). Assessment of the effect of increasing temperature on the ecology and assemblage structure of modern planktic foraminifers in the Caribbean and surrounding seas. Journal of Foraminiferal Research 48 (3), 251–272. doi:10.2113/gsjfr.48.3.251.

Johns, W.E., Townsend, T.L., Fratantoni, D.M., Wilson, W.D. (2002). On the Atlantic inflow to the Caribbean Sea. Deep Sea Research Part I: Oceanographic Research Papers 49 (2), 211–243.

Kameo, K., Shearer, M., Droxler, A., Mita, I., Watanabe, R., Sato, T. (2004). Glacial–interglacial surface water variations in the Caribbean Sea during the last 300 ky based on calcareous nannofossil analysis. Palaeogeography, Palaeoclimatology, Palaeoecology 212 (1-2), 65–76.

Kilbourne, K.H., Quinn, T.M., Guilderson, T.P., Webb, R.S., Taylor, F.W. (2007). Decadal- to interannual-scale source water variations in the Caribbean Sea recorded by Puerto Rican coral radiocarbon. Climate Dynamics 29, 51-62. DOI 10.1007/s00382-007-0224-2.

Kirchner, K., Rhein, M., Hüttl-Kabus, S., Böning, C.W. (2009). On the spreading of South Atlantic Water into the Northern Hemisphere. Journal of Geophysical Research 114 (C5), 363.

Latif, M., Roeckner, E., Mikolajewicz, U., Voss, R. (2000) Tropical stabilization of the thermohaline circulation in a Greenhouse warming simulation. J. Clim. 13, 1809-1813. https://doi.org/10.1175/1520-0442(2000)013<1809:L>2.0.CO;2

Leduc, G., Vidal, L., Tachikawa, K., Rostek, F., Sonzogni, C., Beaufort, L., Bard, E. (2007). Moisture transport across Central America as a positive feedback on abrupt climatic changes. Nature 445. doi:10.1038/nature05578.

Lippold, J., Grützner, J., Winter, D., Lahaye, Y., Mangini, A., Christl, M. (2009). Does sedimentary $^{231}Pa/^{230}Th$ from the Bermuda Rise monitor past Atlantic Meridional Overturning Circulation? Geophysical Research Letters 36, L12601.

Lippold, J., Pöppelmeier, F., Süfke, F., Gutjahr, M., Goepfert, T.J., Blaser, P., Friedrich, O., Link, J.M., Wacker, L., Rheinberger, S., Jaccard, S.L. (2019). Constraining the variability of the Atlantic Meridional Overturning Circulation during the Holocene. Geophysical Research Letters 46 (20), 11338-11346. https://doi.org/10.1029/2019GL084988.

Locarnini, R.A., Mishonov, A.V., Antonov, J.I., Boyer, T.P., Garcia, H.E., Baranova, O. K., Zweng, M.M., Paver, C.R., Reagan, J.R., Johnson, D.R., Hamilton, M., Seidov, D. (2013). World Ocean Atlas 2013, volume1: Temperature. Levitus S, Ed.; Mishonov A, Technical Ed.; NOAA Atlas NESDIS 73, p. 40.

Locarnini, R.A., Mishonov, A.V., Baranova, O.K., Boyer, T.P., Zweng, M.M., Garcia, H.E., Reagan, J.R., Seidov, D., Weathers, K.W., Paver, C.R., Smolyar, I.V. (2018). Temperature. NOAA Atlas NESDIS in preparation. World Ocean Atlas 2018 (1).

Lohmann, G.P., Schweitzer, P.N. (1990). *Globorotalia truncatulinoides'* growth and chemistry as probes of the past thermocline: 1. Shell size. Paleoceanography 5 (1), 55– 75.

Lynch-Stieglitz, J., Schmidt, M.W., Gene Henry, L., Curry, W.B., Skinner, L.C., Mulitza, S., Zhang, R., Chang, P. (2014). Muted change in Atlantic overturning circulation over some glacial-aged Heinrich events. Nature Geoscience 7 (2), 144–150.

McManus, J.F., Francois, R., Gherardi, J.M., Keigwin, L.D., Brown-Leger, S. (2004). Collapse and rapid resumption of Atlantic meridional circulation linked to deglacial climate changes. Nature 428 (6985), 834–837. https://doi.org/10.1038/nature02494.

Mignot, J., Ganopolski, A., Levermann, A. (2007). Atlantic subsurface temperatures: Response to a shutdown of the overturning circulation and consequences for its recovery. Journal of Climate 20 (19), 4884–4898. https://doi.org/10.1175/JCLI4280.1

Ng, H.C., Robinson, L.F., McManus, J.F., Mohamed, K.J., Jacobel, A.W., Ivanovic, R.F., Gregoire, L.J., Chen, T. (2018). Coherent deglacial changes in western Atlantic Ocean circulation. Nature Communications 9, 2947.

NGRIP Dating Group (2006). Greenland Ice Core Chronology 2005 (GICC05): IGBP PAGES/World Data Center for Paleoclimatology. Data Contribution Series # 2006-118, NOAA/NCDC Paleoclimatology Program, Boulder CO, USA.

Nürnberg, D., Ziegler, M., Karas, C., Tiedemann, R., Schmidt, M.W. (2008). Interacting Loop Current variability and Mississippi River discharge over the past 400 kyr. Earth and Planetary Science Letters 272 (1-2), 278-289. https://doi.org/10.1016/j.epsl.2008.04.051.

Nürnberg, D., Böschen, T., Doering, K., Mollier-Vogel, E., Raddatz, J., Schneider, R. (2015). Sea surface and subsurface circulation dynamics off equatorial Peru during the last ~17 kyr. Paleoceanography 30 (7), 984–999.

Nürnberg, D., Riff, T., Bahr, A., Karas, C., Meier, K., Lippold, J. (2020). Stable isotopes and Mg/Ca ratios of *Globorotalia truncatulinoides* from sediment core M78/1_235-1. PANGAEA, https://doi.org/10.1594/PANGAEA.919497.

O'Connor, B.M., Fine, R.A., Olson, D.B. (2005). A global comparison of subtropical underwater formation rates. Deep Sea Research Part I: Oceanographic Research Papers 52 (9), 1569–1590.

Pahnke, K., Goldstein, S.L., Hemming, S.R. (2008). Abrupt changes in Antarctic Intermediate Water circulation over the past 25,000 years. Nature Geoscience 1, 870-773.

Paillard, D., Labeyrie, L., Yiou, P. (1996), Macintosh program performs time-series analysis, Eos Trans. AGU 77, 379.

Parker, A.O., Schmidt, M.W., Chang, P. (2015). Tropical North Atlantic subsurface warming events as a fingerprint for AMOC variability during Marine Isotope Stage 3. Paleoceanography 30 (11), 1425–1436.

Peterson, L.C., Haug, G.H., Hughen, K.A., Röhl, U. (2000). Rapid changes in the hydrologic cycle of the tropical Atlantic during the last glacial. Science (New York, N.Y.) 290 (5498), 1947–1951.

Philander, S.G.H., Pacanowski, R.C. (1986). A model of the seasonal cycle in the tropical Atlantic Ocean. Journal of Geophysical Research 91 (C12), 14192.

Poggemann, D.-W., Hathorne, E.C., Nürnberg, D., Frank, M., Bruhn, I., Reißig, S., Bahr, A. (2017). Rapid deglacial injection of nutrients into the tropical Atlantic via Antarctic Intermediate Water. Earth and Planetary Science Letters 463, 118–126. http://dx.doi.org/10.1016/j.epsl.2017.01.

Poggemann, D.-W., Nürnberg, D., Hathorne, E.C., Frank, M., Rath, W., Reißig, S., Bahr, A. (2018). Deglacial heat Uptake by the Southern Ocean and Rapid Northward Redistribution Via Antarctic Intermediate Water. Paleoceanography and Paleoclimatology 33 (11), 1292–1305. https://doi.org/10.1029/2017PA003284.

Qu, T., Gao, S., Fukumori, I. (2013). Formation of salinity maximum water and its contribution to the overturning circulation in the North Atlantic as revealed by a global general circulation model. Journal of Geophysical Research: Oceans 118 (4), 1982–1994.

Rahmstorf, S. (2003). Timing of abrupt climate change: A precise clock. Geophysical Research Letters 30 (10), 1510. doi:10.1029/2003GL017115.

Repschläger, J., Weinelt, M., Kinkel, H., Andersen, N., Garbe-Schönberg, D., Schwab, C. (2015). Response of the subtropical North Atlantic surface hydrography on deglacial and Holocene AMOC changes. Paleoceanography 30, 456–476. https://doi.org/10.1002/ 2014PA002637.

Reißig, S., Nürnberg, D., Bahr, A., Poggemann, D.-W., Hoffmann, J. (2019). Southward displacement of the North Atlantic subtropical gyre circulation system during North Atlantic cold spells. Paleoceanography and Paleoclimatology 34. https://doi. org/10.1029/2018PA003376.

Rühlemann, C., Mulitza, S., Lohmann, G., Paul, A., Prange, M., Wefer, G. (2004). Intermediate depth warming in the tropical Atlantic related to weakened thermohaline circulation: Combining paleoclimate data and modeling results for the last deglaciation. Paleoceanography 19 (1), PA1025, doi: 10.1029/2003PA000948.

Sarnthein, M., Balmer, S., Grootes, P. M., Mudelsee, M. (2015). Planktic and benthic ^{14}C reservoir ages for three ocean basins, calibrated by a suite of ^{14}C plateaus in the glacial-to-deglacial Suigetsu atmospheric ^{14}C record. Radiocarbon 57 (1), 129–151. https://doi.org/10.2458/azu_rc.57.17916.

Sarnthein, M., Küssner, K., Grootes, P.M., Ausin, B., Eglinton, T., Muglia, J., Muscheler, R., Schlolaut, G. (2019). Plateaus and jumps in the atmospheric radiocarbon record – Potential origin and value as global age markers for glacial-to-deglacial paleoceanography, a synthesis. Climate of the Past. https://doi.org/10.5194/cp-2019-127.

Schlitzer, R. (2015). Ocean data view. [Available at http://odv.awi.de.]

Schmidt, G.A., Bigg, G.R., Rohling, E.J. (1999). Global Seawater Oxygen-18 Database - v1.22. https://data.giss.nasa.gov/o18data.

Schmidt, M.W., Chang, P., Hertzberg, J.E., Them, T.R., Ji, L., J, L., Otto-Bliesner, B.L. (2012). Impact of abrupt deglacial climate change on tropical Atlantic subsurface temperatures. Proceedings of the National Academy of Sciences of the United States of America 109 (36), 14348–14352.

Schmitz, W.J., McCartney, M.S. (1993). On the North Atlantic circulation. Review of Geophysics, 31(1), 29–49. https://doi.org/10.1029/92RG02583.

Schönfeld, J., Bahr, A., Bannert, B., Bayer, A.-S., Bayer, M., Beer, C., Blanz, T., Dullo, W.-C., Flögel, S., Garlichs, T., Haley, B., Hübscher, C., Joseph, N., Kucera, M., Langenbacher, J., Nürnberg, D., Ochsenhirt, W.-T., Petersen, A., Pulm, P., Titschack, J., Troccoli, L. (2011). Surface and Intermediate Water hydrography, planktonic and benthic biota in the Caribbean Sea – Climate, Bio and Geosphere linkages (OPOKA) - Cruise No. M78/1 - February 22 – March 28, 2009 - Colón (Panama) – Port of Spain (Trinidad and Tobago). METEOR-Berichte, 196 p., ISSN 2195-8475.

Schwab, C., Kinkel, H., Weinelt, M., Repschläger, J. (2012). Coccolithophore paleoproductivity and ecology response to deglacial and Holocene changes in the Azores Current System. Paleoceanography 27, PA3210. https://doi.org/10.1029/2012PA002281.

Slowey, N.C., Curry, W.B. (1995). Glacial-interglacial differences in circulation and carbon cycling within the upper western North Atlantic. Paleoceanography 10 (4), 715–732. doi:10.1029/95PA01166.

Stern, J.V., Lisiecki, L.E. (2013). North Atlantic circulation and reservoir age changes over the past 41,000 years. Geophysical Research Letters 40, 3693–3697. https://doi.org/10.1002/grl.50679.

Stuiver, M., Reimer, P.J., and Reimer, R.W., 2020, CALIB 8.2 [WWW program] at http://calib.org, accessed 2020-10-14.

Them, T.R., Schmidt, M.W., Lynch-Stieglitz, J. (2015). Millennial-scale tropical atmospheric and Atlantic Ocean circulation change from the Last Glacial Maximum and Marine Isotope Stage 3. Earth and Planetary Science Letters 427, 47–56.

Thunell, R., Tappa, E., Pride, C., Kincaid, E. (1999). Sea-surface temperature anomalies associated with the 1997–1998 El Niño recorded in the oxygen isotope composition of planktonic foraminifera. Geology 27 (9), 843.

Vellinga, M., Wu, P. (2004). Low-Latitude Freshwater Influence on Centennial Variability of the Atlantic Thermohaline Circulation. Journal of Climate 17 (23), 4498–4511.

Vink, A., Rühlemann, C., Zonneveld, K.A.F., Mulitza, S., Hüls, M., Willems, H. (2001). Shifts in the position of the north equatorial current and rapid productivity changes in the western tropical Atlantic during the last glacial. Paleoceanography 16 (5), 479–490.

Waelbroeck, C., Labeyrie, L., Michel, E., Duplessy, J. C., McManus, J. F., Lambeck, K., et al. (2002). Sea-level and deep water temperature changes derived from benthic foraminifera isotopic records. Quaternary Science Reviews 21 (1–3), 295–305.

Wary, M., Eynaud, F., Sabine, M., Zaragosi, S., Rossignol, L., Malaizé, B., Palis, E., Zumaque, J., Caulle, C., Penaud, A., Michel, E., Charlier, K. (2015). Stratification of surface waters during the last glacial millennial climatic events: a key factor in subsurface and deep-water dynamics. Climate of the Past 11, 1507-1525. doi:10.5194/cp-11-1507-2015.

Wüst, G. (Ed.) (1964). Stratification and Circulation in the Antillean–Caribbean Basins. Part 1, Spreading and Mixing of the Water Types with an Oceanographic Atlas. Columbia University Press, New York.

Zahn, R., Stüber, A. (2002). Suborbital intermediate water variability inferred from paired benthic foraminiferal Cd/Ca and $\delta^{13}C$ in the tropical West Atlantic and linking with North Atlantic climates. Earth and Planetary Science Letters 200 (1-2), 191–205.

Zhang, X., Prange, M., Merkel, U., Schulz, M. (2015). Spatial fingerprint and magnitude of changes in the Atlantic meridional overturning circulation during marine isotope stage 3. Geophysical Research Letters 42 (6), 1903–1911.

Zhang, X., Knorr, G., Lohmann, G., Barker, S. (2017). Abrupt North Atlantic circulation changes in response to gradual CO_2 forcing in a glacial climate state. Nature Geoscience 10. doi:10.1038/NGEO2974.

Zhu, J., Liu, Z., Zhang, X., Eisenman, I., Liu, W. (2014). Linear weakening of the AMOC in response to receding glacial ice sheets in CCSM3. Geophysical Research Letters 41 (17), 6252–6258.

Appendix (Supporting Information) for

Western Boundary Current in relation to Atlantic Subtropical Gyre dynamics during abrupt glacial climate fluctuations

Dirk Nürnberg[1], Tabitha Riff[1], André Bahr[2], Cyrus Karas[3], Karl Meier[2], Jörg Lippold[2]

[1]GEOMAR Helmholtz Centre for Ocean Research Kiel, Wischhofstr. 1-3, D-24148 Kiel, Germany

[2]Institute of Earth Science, Heidelberg University, Im Neuenheimer Feld 234, D-69120 Heidelberg, Germany

[3]Universidad de Santiago, Av. B. O'Higgins 3363, Santiago, Chile

Correspondence to: Dirk Nürnberg (dnuernberg@geomar.de)

Introduction

The following part includes text passages, figures, and data tables supporting the abovementioned study. The text discusses in higher detail the ecology of the selected foraminiferal species, and diverse aspects relevant to the Mg/Ca-paleo thermometry. We also provide support for the observed cyclicity in the $subSST_{Mg/Ca}$-record. We document the age model modifications we made on the reference $subSST_{Mg/Ca}$-dataset of Parker et al. (2015).

1. **Text A.1** (text01.txt) Supporting information on foraminiferal species selected and their ecology, analytical details and error assessment for foraminiferal Mg/Ca, contamination and calcite dissolution issues, and references.
2. **Fig. A.1** (fs01.eps) Seasonal temperatures [°C] and salinities [psu] for the upper ~800 m water depth.
3. **Fig. A.2** (fs02.eps) Stable oxygen and carbon isotope signatures of *G. truncatulinoides* specimens from core 235.
4. **Fig. A.3** (fs03.eps) Comparison of temperature calibrations available for *G. truncatulinoides*.
5. **Fig. A.4** (fs04.eps) Contamination plots.
6. **Fig. A.5** (fs05.eps) Downcore $Mg/Ca_{G. truncatulinoides}$.
7. **Fig. A. 6** (fs06.eps) The frequency spectrum of the core 235 $subSST_{Mg/Ca}$ record.
8. **Fig. A.7.** (fs07.eps) Comparison of Tobago and Bonaire basins $subSST_{Mg/Ca}$ records on consistent chronologies.

9. Table A.1 (ts01.txt) Age control for Tobago Basin core 235 .

Text A.1. Supporting information on foraminiferal species selected and their ecology, analytical details and error assessment for foraminiferal Mg/Ca, contamination and calcite dissolution issues, and references.

Ecology of the selected foraminiferal species

To reconstruct subsurface ocean properties, we selected calcitic tests of the planktonic foraminiferal species *Globorotalia truncatulinoides* (d´Orbigny, 1839). *G. truncatulinoides* is a deep-dwelling, subtropical species, which is adopted to a wide range of water temperatures and salinities (Lohmann and Schweitzer 1990). Its stratigraphic range is from early Pleistocene to today (Kennett and Srinivasan, 1983). *G. truncatulinoides* exhibits a complex life cycle, beginning in the upper meters of the water column. It continues to grow and calcify new chambers at greater water depth until it reaches its adult stage, apparently pursuing a reproductive strategy that requires annual vertical migration of several hundred meters, with greater living depths during spring and summer (Cléroux et al., 2009). Sediment trap time series in the northern Gulf of Mexico demonstrate that 92% of its flux occurs from January to March (Reynolds et al., 2018). In the Atlantic and the Caribbean, the habitat depth range of *G. truncatulinoides* is from 0 m to >400 m) (e.g. Cléroux et al., 2008; Jentzen et al., 2018b; Schmuker and Schiebel, 2002; Steph et al., 2009). Encrustation stages, however, may reflect calcification at different depths (Reynolds et al., 2018). Non-encrusted and encrusted specimens reveal mean calcification depths of 66 ± 9 m (with a range between 0-150 m) and 379 ± 76 m (with a range between 170 and 700 m), respectively (Reynolds et al., 2018). In the eastern Caribbean, *G. truncatulinoides* apparently prefers a habitat at 180-300 m (Jentzen et al., 2018b) (c.f. Fig. A.1).

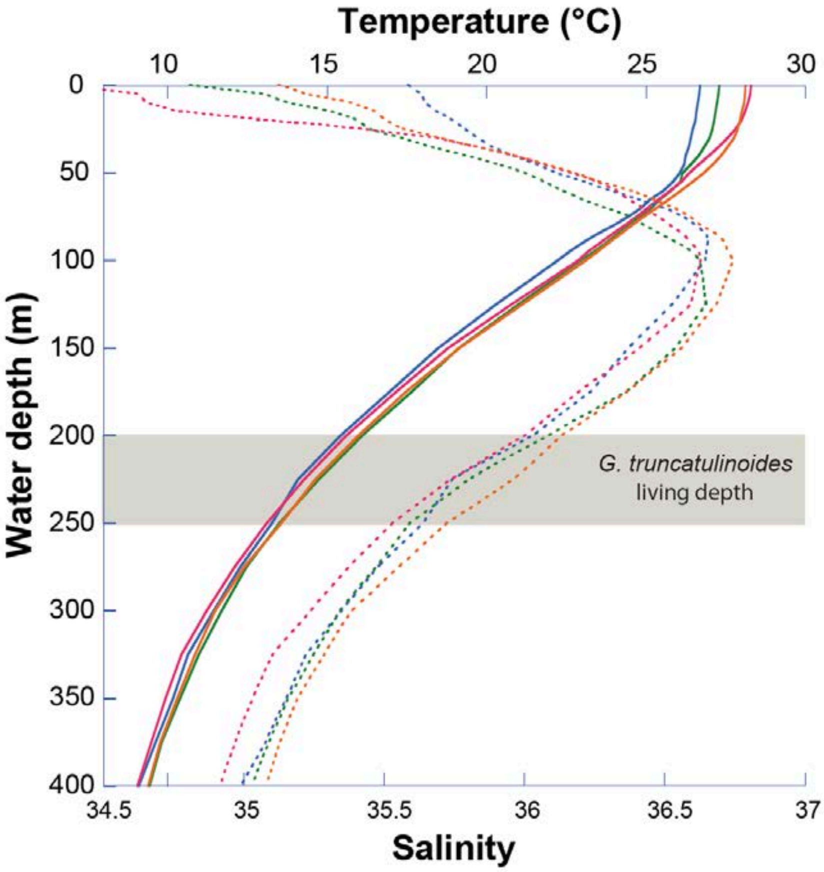

Fig. A.1. Seasonal temperatures [°C] and salinities [psu] for the upper ~800 m water depth (WOA Station 25458 at 11.5°N 60.5°W; Locarnini et al., 2018). Solid and stippled lines denote the temperature and salinity profiles, respectively: Jan.-Mar. (blue), Apr.-Jun. (green), Jul.-Sep. (red), Oct.-Dec. (orange). Gray shading marks the assumed living depth of *G. truncatulinoides* according to Jentzen et al. (2018a).

As the majority of the *G. truncatulinoides* specimens in core 235 are encrusted (c.f. Fig. A.2), and as the core 235 location is closer to the eastern part of the Caribbean, we assume a habitat depth range of ~200-250 m. This corresponds to a depth nearly below the main thermocline in Tobago Basin (180-220 m) (Locarnini et al., 2018) and is in good agreement with the findings of Jentzen et al. (2018b).

G. truncatulinoides shows a coiling dimorphism, separating this species into sinistral (left-coiled) and dextral (right-coiled) morphotypes. The preferred habitats of both morphotypes, however, are rather similar (Jentzen et al., 2018b; Cléroux et al., 2008). Following Friedrich et al. (2012) and Ganssen and Kroon (2000), who showed that both morphotypes have similar stable oxygen isotopic ($\delta^{18}O$), carbon isotopic ($\delta^{13}C$) and Mg/Ca signatures, we did not differentiate between coiling directions. Ujiié et al. (2010) further showed that the dextral form is dominant at our core 235 location.

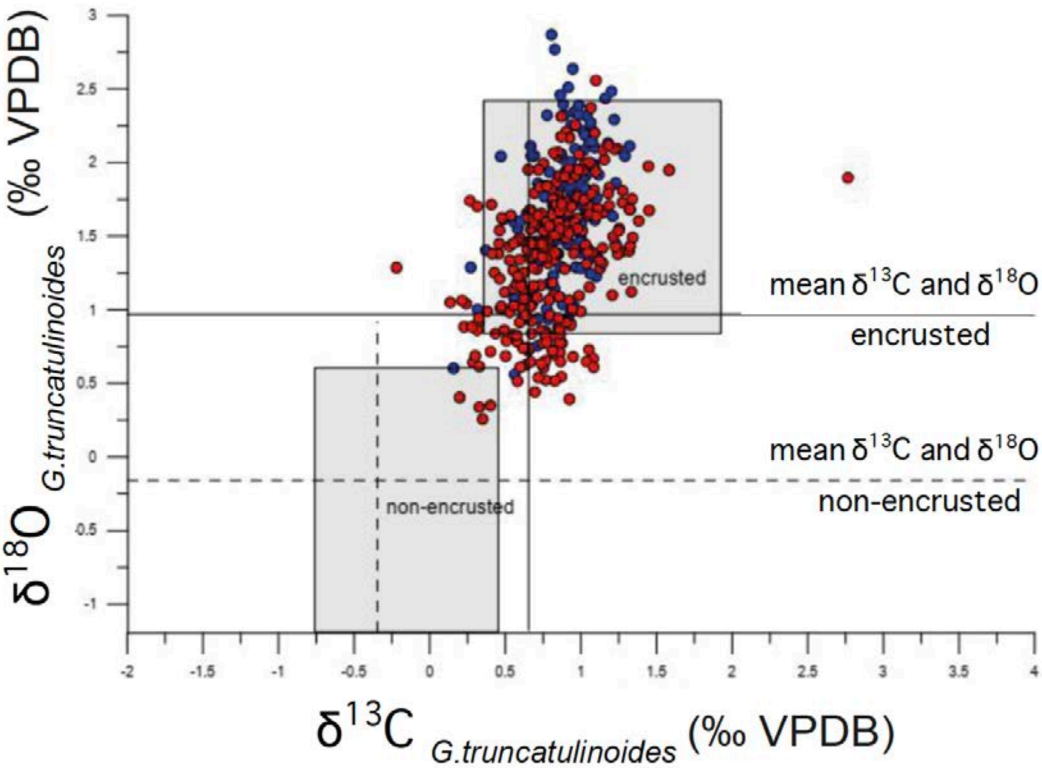

Fig. A.2. Stable oxygen and carbon isotope signatures of *G. truncatulinoides* specimens from core 235. The $\delta^{13}C$ and $\delta^{18}O$ data (in ‰ vs. VPDB) of this study are in blue, while the associated Reißig et al. (2019) data are in red, all measured on the same mass spectrometer (c.f. Chapter 3.3.1). The gray shaded fields denote data ranges and means for either encrusted or non-encrusted specimens (Reynolds et al., 2018). In this study, most specimens selected for geochemical analyses are encrusted individuals.

Calcitic tests of the foraminiferal species were hand-picked under a binocular microscope. The size fraction had to be enlarged to 250-400 µm due to insufficient sample material. Friedrich et al. (2012) stated that *G. truncatulinoides* has no size effect on Mg/Ca. Also, $\delta^{13}C$ and $\delta^{18}O$ show no systematic changes in the selected size fraction (Elderfield et al. 2002). For the isotope-geochemical studies, ~30 species-specific foraminiferal tests per sample were gently crushed between cleaned glass plates to open the chambers for efficient cleaning. Over-crushing was avoided to prevent an excessive sample loss during cleaning procedure. The fragments of the tests were homogenized and split into subsamples for stable isotope (one third) and trace metal analyses (two thirds) and transferred into cleaned vials. Chamber fillings (e.g. pyrite, clay) and other contaminant phases (e.g. conglomerates of metal oxides) were thoroughly removed before chemical cleaning and analyses. All analytical data are available online at the Data Publisher for Earth and Environmental Science, PANGEA (www.pangaea.de): https://doi.org/10.1594/PANGAEA.919497.

Foraminiferal Mg/Ca-paleo thermometry

Over the past decades, foraminiferal Mg/Ca has been proven to be a robust, reliably precise, and reproducible proxy for ocean temperatures (e.g., Elderfield and Ganssen, 2000; Lea et al., 1999; Nürnberg, 1995, 2000; Nürnberg et al., 1996). To prepare the foraminiferal samples for elemental analyses, the foraminiferal tests were intensively cleaned oxidatively and reductively (with hydrazine) following the protocols from Boyle and Keigwin (1985/86) and Boyle and Rosenthal (1996). This procedure was similarly applied by Reißig et al. (2019) on core 235 foraminiferal sample material, and allows direct comparison of analytical results. Trace metal analyses were performed on a VARIAN 720-ES Axial ICP-OES, a simultaneous, axial-viewing Inductively Coupled Plasma - Optical Emission Spectrometer coupled to a VARIAN SPS3 sample preparation system. To assure analytical quality control the measurement strategy involved the regular analyses of standards and blanks. The results were normalized to the ECRM 752-1 standard (3.761 mmol/mol Mg/Ca; Greaves et al., 2008) and were drift corrected. The external reproducibility for the ECRM standard was ±0.01 mmol/mol for Mg/Ca (2σ SD). Replicate measurements reveal a reproducibility of ±0.28 mmol/mol for *G. truncatulinoides* (2σ SD).

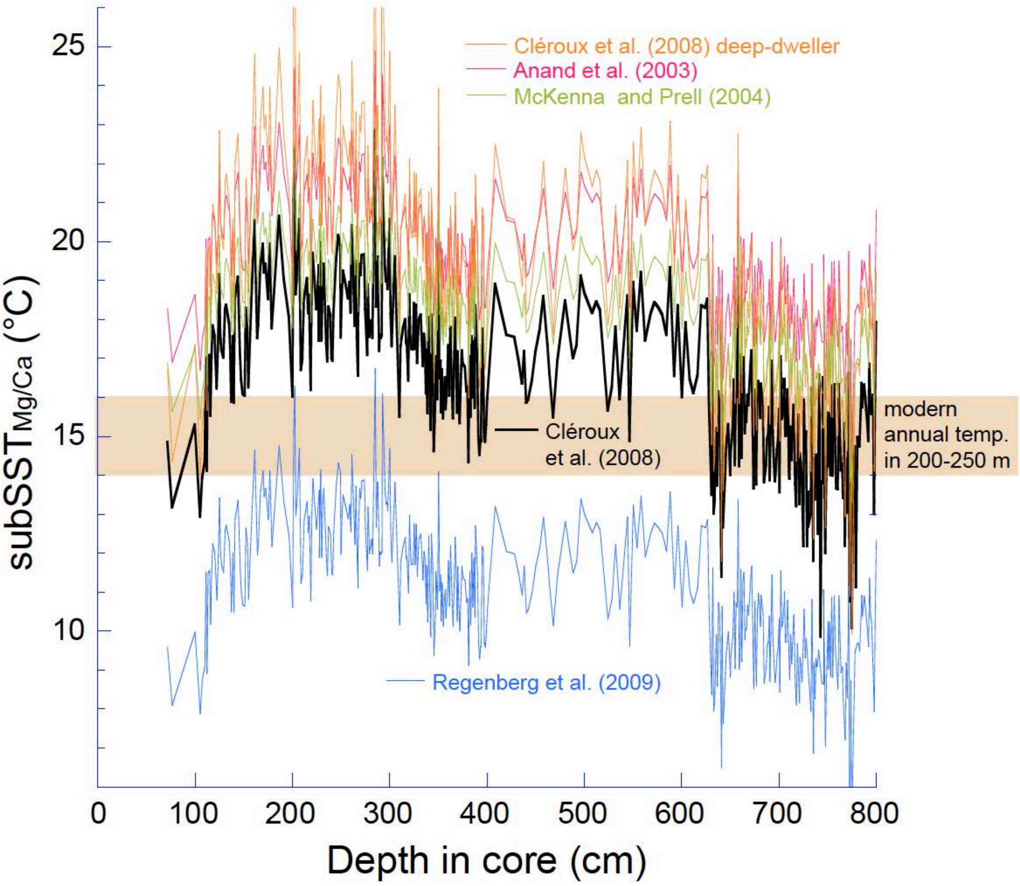

Fig. A.3. Comparison of temperature calibrations available for *G. truncatulinoides*. Calibrations of Cléroux et al. (2008) (dextral morphotype) and Cléroux et al. (2008) (deep-dweller) were considered most reliable (black and orange) to convert Mg/Ca$_{G.truncatulinoides}$ into subSST$_{Mg/Ca}$. Other calibrations from Anand (2003; red), Regenberg et al. (2009; blue; deep-dweller) and McKenna and Prell (2004; green) were not applied, as they provide too warm or too cool core-top subSST$_{Mg/Ca}$. Brown-shading indicates modern annual temperatures at 200-250m water depth in Tobago Basin (c.f. Fig. A.1).

For *G. truncatulinoides*, there is a variety of calibration equations available to convert the foraminiferal Mg/Ca ratios into paleotemperatures (c.f. Fig. A.3). The Mg/Ca$_{G.truncatulinoides}$ ratios were converted into subsurface temperatures (termed subSST$_{Mg/Ca}$) using the exponential calibration equation of Cléroux et al. (2008) established from widely distributed Atlantic sample material: Mg/Ca = 0.62 $\pm$ 0.16 exp(0.74 $\pm$ 0.017 * T). We finally applied the calibration for the dextral morphotype (s. above). When applying the calibration equation of Cléroux et al. (2008), the calculated latest Holocene subSST$_{Mg/Ca}$ of ~14.9°C (Reißig et al.,

2019) matches the modern annual subsurface temperatures of 14-15°C at 200-250 m depth (Locarnini et al., 2018). With the asserted reproducibility of 0.28 mmol/mol, the error (2σ) of calculated $subSST_{Mg/Ca}$ is ± 0.71°C. In order to achieve consistency between our datasets and published reference datasets from Bonaire Basin, we recalculated the Parker et al. (2015) $subSST_{Mg/Ca}$ data derived from $Mg/Ca_{\textit{G.truncatulinoides}}$ ratios using the Cléroux et al. (2008) calibration. This led to consistently lower-by-4°C $subSST_{Mg/Ca}$ for the glacial time period then previously published by Parker et al. (2015), who used the Anand et al. (2003) calibration. Reißig et al. (2019) in detail discussed the appropriateness of the Cléroux et al. (2008) calibration.

Analytical outliers and contamination effects

A small number of single trace metal analyses from 670 cm, 683 cm, 714 cm, 755.5 cm, 763 cm and 770.5 cm core depths were removed from the core 235 dataset as they yielded extremely high/low element/Ca values compared with the surrounding data, and the according Mg/Ca data led to unrealistically high or low $subSST_{Mg/Ca}$ values. The Mg/Ca data (2.65, 0.88, 4.14, 1.99, 1.29, 1.28 mmol/mol) were accompanied by high Al/Ca (0.7, 0.12, 0.49, 1.14, 0.94, 2.34 mmol/mol) and Fe/Ca (0.18, 0.06, 0.16, 0.27, 3.39, 0.03 mmol/mol) ratios, (c.f. Fig. A.4).

By monitoring the remaining foraminiferal samples for their Fe/Ca, Al/Ca and Mn/Ca ratios, the effect of cleaning efficiency, post depositional contamination, and diagenetic alteration on foraminiferal Mg/Ca was examined. Contamination-indicative threshold values exist for Fe/Ca, Al/Ca and Mn/Ca ratios (<0.1 mmol/mol; Barker et al., 2003; Them et al., 2015). Numerous studies have shown meanwhile that the Barker et al. (2003) threshold values - defined in the North Atlantic - are often exceeded as they largely depend on the sediment type the foraminiferal tests were removed from (Nünberg et al., 2015). The Al/Ca, Fe/Ca and Mn/Ca ratios in our foraminiferal samples are often higher than the given threshold values, and at times reach values of up to ~1.1 mmol/mol, ~0.7 mmol/mol, and ~0.22 mmol/mol, respectively (Fig. A.4, A.5). It needs to be noted, in this respect, that these high contaminant values do not consistently have extraordinary foraminiferal Mg/Ca ratios. Also, the correlation of Mg/Ca to either Fe/Ca, Al/Ca or Mn/Ca (R^2 = 0.15, R^2 = 0.19; R^2 = 0.06) is insignificant, suggesting that samples were not contaminated. A high covariance between Mg/Ca and Mn/Ca, Fe/Ca and/or Al/Ca would imply insufficient clay removal during cleaning (Barker et al., 2003).

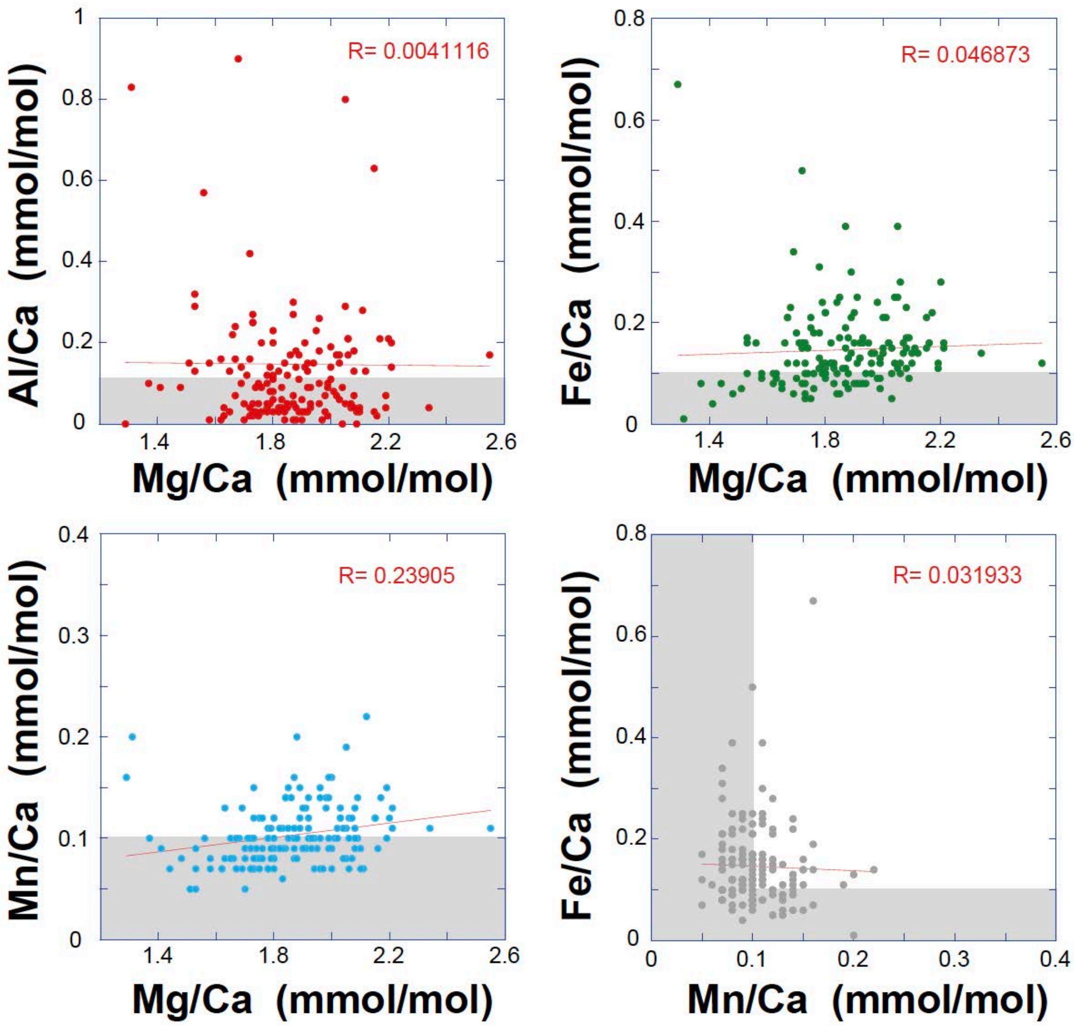

Fig. A.4. Contamination plots. Foraminiferal Mg/Ca vs. Al/Ca (red), Fe/Ca (green), Mn/Ca (blue) reveal only low correlation coefficients (R) for *G. truncatulinoides*. Al/Ca, Fe/Ca and Mn/Ca partly exceed threshold values (>0.1 mmol/mol, gray shading) proposed by Barker et al. (2003). Mn/Ca vs. Fe/Ca is not correlated, implying no ferromanganese coating.

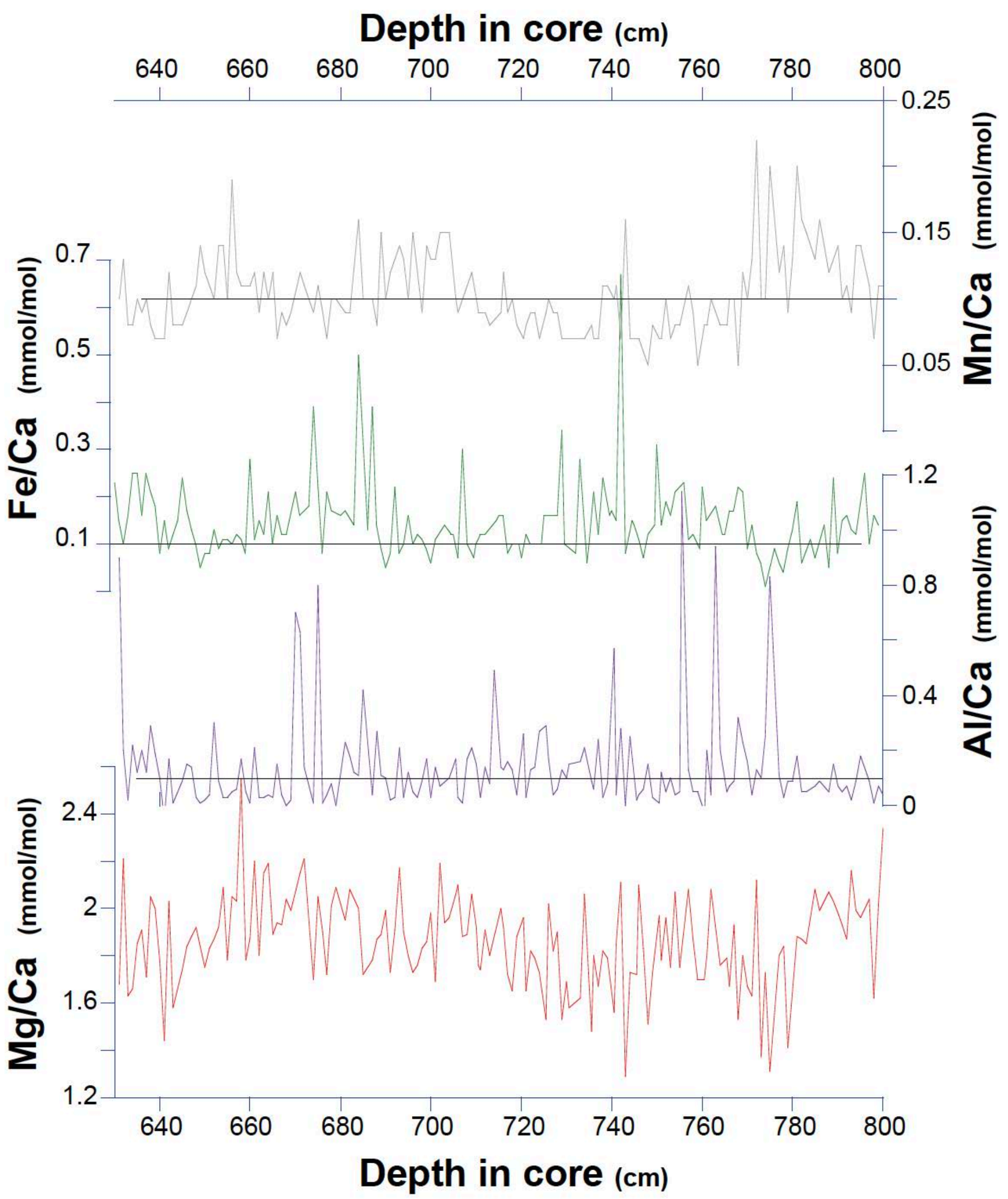

Fig. A.5. Downcore Mg/Ca$_{G.truncatulinoides}$ of Tobago Basin core 235 (red) in comparison to contaminant elemental ratios Al/Ca (blue), Fe/Ca (green), and Mn/Ca (gray) from the same samples. Correlation coefficients are given in Fig. A4. Threshold values indicative of sample contamination (>0.1 mmol/mol) suggested by Barker et al. (2003) and Them et al. (2015) are indicated by horizontal dashed lines, but should be viewed cautiously.

Furthermore, there is no indication that the record of *G. truncatulinoides* is contaminated by Fe-Mn-coatings, which have effects on Mg/Ca. There is no statistically significant positive correlation between Mn/Ca and Fe/Ca (Fig. A.4). Also, foraminiferal samples showing particularly high Mn/Ca ratios are rather low in Fe/Ca (Fig. A.5) suggesting that the foraminiferal Mg/Ca values are not biased by Fe/Mn coatings. According to Roberts et al. (2016), a foraminiferal Mg/Mn ratio of 0.1 mol/mol within a diagenetic coating would account for 10^{-2} mmol/mol at maximum to foraminiferal Mg/Ca, which is well within the reproducibility of the Mg/Ca analyses. In our dataset, the Mg/Mn within foraminiferal tests is on average 0.02±0.005 mol/mol). We hence conclude that sample contamination due to diagenetic coatings is negligible to our Mg/Ca analyses.

When cracking the foraminiferal tests, partially golden to silver colored crystalline particles at the inner chamber walls were observed. These crystalline particles were identified as pyrite (FeS_2), which forms in marine sediments by the activity of sulphate-reducing bacteria under suboxic conditions. Elevated Fe/Ca ratios may reflect the presence of pyrite during the measurements, although brushing of test walls before cleaning, and the intense cleaning steps including nitric acid, to which pyrite is soluble, were considered sufficient enough to remove most of the pyrite coatings. Nürnberg et al. (2015) concluded from samples with high pyrite content from off Peru that even the measured high Fe/Ca ratios (4.08 mmol mol^{-1}) did not affect the Mg/Ca signal.

Dissolution effects on foraminiferal Mg/Ca

It is important to rule out calcite dissolution effects on foraminiferal Mg/Ca, preferentially controlled by the calcite-saturation state of the bottom waters. Regenberg et al. (2006) showed that Mg/Ca starts to decline linearly below $\Delta[CO_3^{2-}]$ levels of ~18- 26 µmol/kg. Later, Regenberg et al. (2014) defined a global critical threshold for dissolution of 21.3 ± 6.6 µmol/kg $\Delta[CO_3^{2-}]$. In Tobago Basin, this threshold value is at a depth of ~3500 m (Regenberg et al., 2014). As core 235 is from ~825 m water depth we assess calcite dissolution unlikely to have affected foraminiferal Mg/Ca. Further discussions on this issue can be found in Poggemann et al. (2017; 2018) and Reißig et al. (2019).

Spectral analysis of subSST$_{Mg/Ca}$ >32.8 ka BP

Based on the established age model, we observe that the highly-variable subSST$_{Mg/Ca}$-record >32.8 ka BP does not follow the D/O-related stadial-interstadial variability. The proxy record, however, is characterized by high-frequency variations, and subSST$_{Mg/Ca}$-maxima occur during stadials and during transitional periods (Fig. 4B). In order to test whether these variations are cyclic, we ran a B-Tukey test (AnalySeries 2.0; Paillard et al., 1996) on the subSST$_{Mg/Ca}$-record >32.8. The according core section from 631 cm to 800 cm core depth showing a sedimentation rate of ~62 cm/kyr was sampled each 1 cm, providing an average temporal resolution of ~20 (+/-15) years of the proxy-record. Dominant ~740 year-cycles were revealed in the B-Tukey frequency spectrum of the 5 point-smoothed subSST$_{Mg/Ca}$ record (Fig. 4B; Fig. A.6) (using a Bartlett window; bandwidth = 0.00110327; error on the power spectrum is 0.511144 < ΔPower / Power < 3.00024). This periodicity not only suggests a regular pacing of the tropical West Atlantic ocean system. It also corroborates the validity of our core chronology, as the ~740 year-periodicity is half of the well-known Dansgaard-Oeschger cycles of 1.470 years (Rahmstorf, 2003).

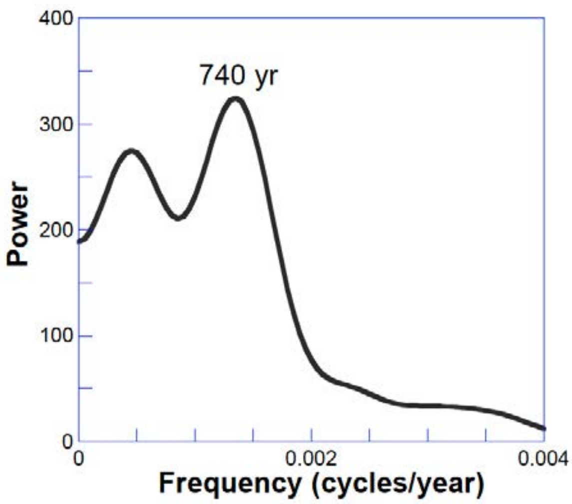

Fig. A. 6. The frequency spectra of the core 235 subSST$_{Mg/Ca}$ record from 37-32.8 ka BP (Fig. 4B) reveals a dominant cyclicity of 740 years, which is half a Dansgaard-Oeschger cycle.

Modified age model for reference core VM12-107 from Bonaire Basin for better comparison

In our study, we attempted to achieve a convincing comparison between our Tobago Basin core 235 $subSST_{Mg/Ca}$ record to a similar record of adjacent Bonaire Basin core VM12-107 (Parker et al., 2015). Although both are well-dated records on D/O stadial/interstadial timescales, the comparison is complicated by the fact that the core 235 AMS^{14}C-chronology is based on the new MARINE20 marine reservoir correction database (Stuiver et al., 2020; http://calib.org), while that of core VM12-107 is not. We hence re-calibrated the AMS^{14}C-datings of core VM12-107 (Parker et al., 2015; Schmidt et al., 2012) by using MARINE20, and by applying a reservoir age correction of -130 $\pm$ 55 years (Hughen et al., 2004) valid for nearby Caraico Basin. The deviation in initial and modified age models is within decades, but allows a better comparison to the core 235 age model in particular for the time period of rapid D/O stadial-interstadial change from 37-30 ka BP (Fig. A.7).

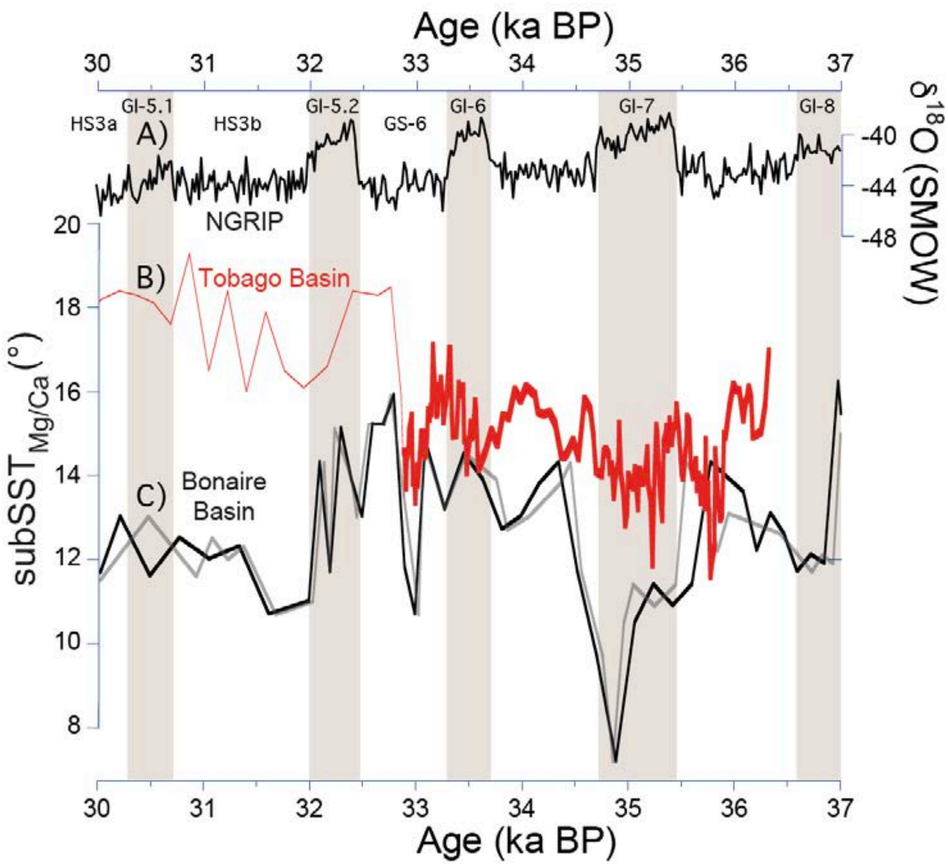

Fig. A.7. Comparison of Tobago and Bonaire basins subSST$_{Mg/Ca}$ records on consistent chronologies. A) Greenland ice core $\delta^{18}O$ record as reference for the northern hemisphere climate signal (NGRIP Dating Group, 2006). B) subSST$_{Mg/Ca}$ record from Tobago Basin (this study). C) subSST$_{Mg/Ca}$ record from Bonaire Basin on the original (Parker et al., 2015; gray) and on the revised age model (this study; black). In order to guarantee compatibility to core 235, the initial AMS^{14}C-datings (31960 yr BP, 33060 yr BP, 35690 yr BP) of Parker et al. (2015) were re-calibrated using the new MARINE20 dataset (Stuiver et al., 2020). The AMS^{14}C-datings were changed to 31872 yr BP, 33073 yr BP, and 35949 yr BP, applying a reservoir age of ΔR = -130 ± 55 years (Hughen et al., 2004; www.calib.org) taken from nearby Caraico Basin.

Table A.1. Age control for Tobago Basin core 235. The age model is primarily based on the linear interpolation between Accelerator Mass Spectrometry (AMS) radiocarbon (^{14}C) dates, analyzed by Cologne AMS (Germany) (Reißig et al., 2019), by Beta Analytic Radiocarbon Dating Laboratory (UK) (Hoffmann et al., 2014; Poggemann et al., 2017), and at the University of Bern following the methodology described by Gottschalk et al. (2018) (this study). Calibrated AMS^{14}C ages using Calib 7.1 software and the new MARINE20 database were calculated by taking in consideration a local reservoir age of 550 yrs (ΔR= -161 ± 24 yrs; Stuiver et al., 2020; http://calib.org). The previously published AMS^{14}C ages (in brackets, black) were still calibrated with MARINE13. Further improvement of the age model was derived by graphically tuning the benthic $\delta^{18}O_{Uvigerina}$ record of core 235 to the high-resolution North Greenland Ice core Project (NGRIP) $\delta^{18}O$ reference record (NGRIP Dating Group, 2006). Thereby, two additional tielines became necessary in order to improve the match of benthic $\delta^{18}O_{Uvigerina}$ minima and Greenland stadials (c. f. Fig. 2).

Core 235 Depth (cm)	**Lab code AMS^{14}C**	**^{14}C Age (yrs BP)**	**Age error +/- (yrs)**	**Median probab. (yrs BP)**	**Remark**	**Lower range (yrs BP)**	**Upper range (yrs BP)**	**Error 1σ (yrs)**	**Lower range (yrs BP)**	**Upper range (yrs BP)**	**Error 2σ (yrs)**	**POINTER age (yrs BP)**	**Refe-rence-**
3	COL147 3.1.1	569	31	185 (242)	AMS^{14}C	110	273	163	0	313	313	**225**	Hoffmann et al. 2014
43	COL147 4.1.1	2926	32	2719 (2732)	AMS^{14}C	2643	2797	154	2530	2868	338	**2719**	Hoffmann et al. 2014
133	COL147 5.1.1	8424	44	9036 (9063)	AMS^{14}C	8935	9137	202	8824	9255	431	**9131**	Hoffmann et al. 2014
188	COL147 6.1.1	10500	48	11820 (11757)	AMS^{14}C	11694	11940	246	11558	12092	534	**11795**	Hoffmann et al. 2014
218	COL147 7.1.1	11586	48	13068 (13103)	AMS^{14}C	12983	13156	173	12880	13240	360	**13119**	Hoffmann et al. 2014
298	COL147 8.1.1	13098	49	15115 (15158)	AMS^{14}C	14996	15229	233	14873	15358	485	**15220**	Hoffmann et al. 2014
317	BETA-453718	12920	40	14881	not consi-dered	14771	15023	252	14575	15118	543		this study
326		13850	60	16098 (16213)	AMS^{14}C	15967	16233	266	15818	16365	547	**16018**	Poggemann et al. 2017
358	COL147 9.1.1	15959	57	18624 (18832)	AMS^{14}C	18518	18765	247	18323	18828	505	**18667**	Poggemann et al. 2017
423	COL148 0.1.1	20139	93	23475 (23793)	AMS^{14}C	23332	23664	332	23147	23756	609	**23447**	Poggemann et al. 2017
614				31999	tie line							**31999**	this study
628		29300	200	33070 (33122)	AMS^{14}C	32793	33399	606	32331	33652	1321	**32845**	Reißig et al. 2019
697	BE-10333.1 .1	29471	228	33286 (33297)	AMS^{14}C	33003	33605	602	32623	33920	1297	**33596**	Reißig et al. 2019
762	BE-10334.1 .1	29881	237	33734	not consi-dered	33475	34031	556	33166	34230	1064		this study
717				34748	tie line							**34748**	this study
795	BE-10335.1 .1	32637	331	36456 (33156)	AMS^{14}C	36091	36821	730	35703	37260	1557	**36172**	this study

References

Anand, P., Elderfield, H., Conte, M.H. (2003). Calibration of Mg/Ca thermometry in planktonic foraminifera from a sediment trap time series. Paleoceanography 18(2), 1050. https://doi.org/10.1029/2002PA000846.

Barker, S., Greaves, M., Elderfield, H. (2003). A study of cleaning procedures used for foraminiferal Mg/Ca paleo thermometry. Geochemistry, Geophysics, Geosystems 4 (9). https://doi.org/10.1029/2003GC000559.

Boyle, E.A., Keigwin, L.D. (1985/86). Comparison of Atlantic and Pacific paleochemical records for the last 215,000 years: changes in deep ocean circulation and chemical inventories. Earth Planetary Science Letters 76, 135-150.

Boyle, E.A., Rosenthal, Y. (1996). Chemical hydrography of the South Atlantic during the Last Glacial Maximum: Cd vs. $\delta^{13}C$. In: Wefer, G., Berger, W.H., Siedler, G., Webb, D. (eds.), The South Atlantic: Present and Past Circulation, Springer, Berlin, Heidelberg, 423-443.

Cléroux, C., Cortijo, E., Anand, P., Labeyrie, L., Bassinot, F., Caillon, N., Duplessy, J.-C. (2008). Mg/Ca and Sr/Ca ratios in planktonic foraminifera: Proxies for upper water column temperature reconstruction. Paleoceanography 23, PA3214. https://doi.org/10.1029/2007PA001505.

Cléroux, C., Lynch-Stieglitz, J., Schmidt, M.W., Cortijo, E., Duplessy, J.-C. (2009). Evidence for calcification depth change of *Globorotalia truncatulinoides* between deglaciation and Holocene in the Western Atlantic Ocean. Marine Micropaleontology 73 (1-2), 57–61.

Elderfield, H., Ganssen, G. (2000). Past temperature and $\delta^{18}O$ of surface ocean waters inferred from foraminiferal Mg/Ca ratios. Nature 405 (6785), 442–445.

Elderfield, H., Vautravers, M., Cooper, M. (2002). The relationship between shell size and Mg/Ca, Sr/Ca, $\delta^{18}O$, and $\delta^{13}C$ of species of planktonic foraminifera. Geochemistry, Geophysics, Geosystems 3 (8), 1–13.

Friedrich, O., Schiebel, R., Wilson, P.A., Weldeab, S., Beer, C.J., Cooper, M.J., Fiebig, J. (2012). Influence of test size, water depth, and ecology on Mg/Ca, Sr/Ca, $\delta^{18}O$ and $\delta^{13}C$ in nine modern species of planktic foraminifers. Earth and Planetary Science Letters 319- 320, 133–145.

Ganssen, G., Kroon, D. (2000). The isotopic signature of planktonic foraminifera from NE Atlantic surface sediments: Implications for the reconstruction of past oceanic conditions. Journal of the Geological Society 157 (3), 693–699.

Greaves, M., Caillon, N., Rebaubier, H., Bartoli, G., Bohaty, S., Cacho, I., Clarke, L., Cooper, M., Daunt, C., Delaney, M., deMenocal, P., Dutton, A., Eggins, S., Elderfield, H., Garbe- Schoenberg, D., Goddard, E., Green, D., Groeneveld, J., Hastings, D., Hathorne, E., Kimoto, K., Klinkhammer, G., Labeyrie, L., Lea, D.W., Marchitto, T., Martínez-Botí, M.A., Mortyn, P.G., Ni, Y., Nürnberg, D., Paradis, G., Pena, L., Quinn, T., Rosenthal, Y., Russell, A., Sagawa, T., Sosdian, S., Stott, L., Tachikawa, K., Tappa, E., Thunell, R., Wilson, P.A. (2008). Interlaboratory comparison study of calibration standards for foraminiferal Mg/Ca thermometry. Geochemistry, Geophysics, Geosystems 9 (8). https://doi.org/10.1029/2008GC001974.

Gottschalk, J., Szidat, S., Michel, E., Mazaud, A., Salazar, G., Battaglia, M., Lippold, J., Jaccard, S. (2018). Radiocarbon measurements of small-size foraminiferal samples with the Mini Carbon Dating System (MICADAS) at the University of Bern: Implications for paleoclimate reconstructions. Radiocarbon 60(2), 469-491. https://doi.org/10.1017/RDC.2018.3.

Hoffmann, J., Bahr, A., Voigt, S., Schönfeld, J., Nürnberg, D., Rethemeyer, J. (2014). Disentangling abrupt deglacial hydrological changes in northern South America: Insolation versus oceanic forcing. Geology 42 (7), 579–582.

Hughen, K.A, Southon, J.R, Bertrand, C.J.H, Frantz, B., Zermeno, P. (2004). Cariaco Basin calibration update: revisions to calendar and ^{14}C chronologies for core PL07-58PC. Radiocarbon 46, 1161-1187.

Jentzen, A., Nürnberg, D., Hathorne, E. C., Schönfeld, J. (2018a). Mg / Ca and $\delta^{18}O$ in living planktic foraminifers from the Caribbean, Gulf of Mexico and Florida Straits. Biogeosciences 15 (23), 7077-7095. doi:10.5194/bg-15-7077-2018.

Jentzen, A., Schönfeld, J., Schiebel, R. (2018b). Assessment of the effect of increasing temperature on the ecology and assemblage structure of modern planktic foraminifers in the Caribbean and surrounding seas. Journal of Foraminiferal Research 48 (3), 251–272. doi:10.2113/gsjfr.48.3.251.

Kennett, J.P., Srinivasan, M.S. (1983). Neogene planktonic foraminifera. A phylogenetic atlas. Hutchinson Ross, Stroudsburg, Pa.

Lea, D.W., Mashiotta, T.A., Spero, H.J. (1999). Controls on magnesium and strontium uptake in planktonic foraminifera determined by live culturing. Geochimica et Cosmochimica Acta 63 (16), 2369–2379.

Locarnini, R.A., Mishonov, A.V., Baranova, O.K., Boyer, T.P., Zweng, M.M., Garcia, H.E., Reagan, J.R., Seidov, D., Weathers, K.W., Paver, C.R., Smolyar, I.V. (2018). Temperature. NOAA Atlas NESDIS in preparation. World Ocean Atlas 2018 (1).

Lohmann, G.P., Schweitzer, P.N. (1990). *Globorotalia truncatulinoides'* growth and chemistry as probes of the past thermocline: 1. Shell size. Paleoceanography 5 (1), 55– 75.

McKenna, VS; Prell, WL (2004). Calibration of the Mg/Ca of *Globorotalia truncatulinoides* (R) for the reconstruction of marine temperature gradients. Paleoceanography 19(2), PA2006.

https://doi.org/10.1029/2000PA000604.

NGRIP Dating Group (2006). Greenland Ice Core Chronology 2005 (GICC05): IGBP PAGES/World Data Center for Paleoclimatology. Data Contribution Series # 2006- 118,NOAA/NCDC Paleoclimatology Program, Boulder CO, USA.

Nürnberg, D. (1995). Magnesium in tests of *Neogloboquadrina pachyderma* sinistral from high northern and southern latitudes. Journal of Foraminiferal Research 25 (4), 350– 368.

Nürnberg, D. (2000). PALEOCLIMATE: Taking the Temperature of Past Ocean Surfaces. Science (New York, N.Y.) 289 (5485), 1698–1699.

Nürnberg, D., Bijma, J., Hemleben, C. (1996). Assessing the reliability of magnesium in foraminiferal calcite as a proxy for water mass temperatures. Geochimica et Cosmochimica Acta 60 (5), 803–814.

Nürnberg, D., Böschen, T., Doering, K., Mollier-Vogel, E., Raddatz, J., Schneider, R. (2015). Sea surface and subsurface circulation dynamics off equatorial Peru during the last ~17 kyr. Paleoceanography 30 (7), 984–999.

Paillard, D., Labeyrie, L., Yiou, P. (1996), Macintosh program performs time-series analysis, Eos Trans. AGU 77, 379.

Parker, A.O., Schmidt, M.W., Chang, P. (2015). Tropical North Atlantic subsurface warming events as a fingerprint for AMOC variability during Marine Isotope Stage 3. Paleoceanography 30 (11), 1425–1436.

Poggemann, D.-W., Hathorne, E.C., Nürnberg, D., Frank, M., Bruhn, I., Reißig, S., Bahr, A. (2017). Rapid deglacial injection of nutrients into the tropical Atlantic via Antarctic Intermediate Water. Earth and Planetary Science Letters 463, 118–126. http://dx.doi.org/10.1016/j.epsl.2017.01.

Poggemann, D.-W., Nürnberg, D., Hathorne, E.C., Frank, M., Rath, W., Reißig, S., Bahr, A. (2018). Deglacial Heat Uptake by the Southern Ocean and Rapid Northward Redistribution Via Antarctic Intermediate Water. Paleoceanography and Paleoclimatology 33 (11), 1292–1305. https://doi.org/10.1029/2017PA003284.

Rahmstorf, S. (2003). Timing of abrupt climate change: A precise clock. Geophysical Research Letters 30 (10), 1510. doi:10.1029/2003GL017115.

Regenberg, M., Nürnberg, D., Steph, S., Groeneveld, J., Garbe-Schönberg, D., Tiedemann, R., Dullo, W.-C. (2006). Assessing the effect of dissolution on planktonic foraminiferal Mg/Ca ratios: Evidence from Caribbean core tops. Geochemistry, Geophysics, Geosystems 7 (7), Q07P15. doi:10.1029/2005GC001019.

Regenberg, M., Steph, S., Nürnberg, D., Tiedemann, R., Garbe-Schönberg, D. (2009). Calibrating Mg/Ca ratios of multiple planktonic foraminiferal species with $\delta^{18}O$-calcification temperatures: Paleothermometry for the upper water column. Earth and Planetary Science Letters 278, 324–336.

Regenberg, M., Regenberg, A., Garbe-Schönberg, D., Lea, D.W. (2014). Global dissolution effects on planktonic foraminiferal Mg/Ca ratios controlled by the calcite-saturation state of bottom waters. Paleoceanography 29, 127–142. doi:10.1002/2013PA002492.

Reißig, S., Nürnberg, D., Bahr, A., Poggemann, D.-W., Hoffmann, J. (2019). Southward displacement of the North Atlantic subtropical gyre circulation system during North Atlantic cold spells. Paleoceanography and Paleoclimatology 34. https://doi. org/10.1029/2018PA003376.

Reynolds, C.E., Richey, J.N., Fehrenbacher, J.S., Rosenheim, B.E., Spero, H.J. (2018). Environmental controls on the geochemistry of *Globorotalia truncatulinoides* in the Gulf of Mexico: Implications for paleoceanographic reconstructions. Marine Micropaleontology 142, 92–104.

Roberts, J., Gottschalk, J., Skinner, L.C., Peck, V.L., Kender, S., Elderfield, H., Waelbroeck, C., Vázquez Riveiros, N., Hodell, D.A. (2016). Evolution of South Atlantic density and chemical stratification across the last deglaciation. Proceedings of the National Academy of Sciences of the United States of America 113 (3), 514–519.

Schmidt, M.W., Chang, P., Hertzberg, J.E., Them, T.R., Ji, L., J, L., Otto-Bliesner, B.L. (2012). Impact of abrupt deglacial climate change on tropical Atlantic subsurface temperatures. Proceedings of the National Academy of Sciences of the United States of America 109 (36), 14348–14352.

Schmuker, B., Schiebel, R. (2002). Planktic foraminifers and hydrography of the eastern and northern Caribbean Sea. Marine Micropaleontology 46 (3-4), 387–403.

Steph, S., Regenberg, M., Tiedemann, R., Mulitza, S., Nürnberg, D. (2009). Stable isotopes of planktonic foraminifera from tropical Atlantic/Caribbean core-tops: Implications for reconstructing upper ocean stratification. Marine Micropaleontology 71 (1-2), 1–19. https://doi.org/10.1016/j.marmicro.2008.12.004.

Stuiver, M., Reimer, P.J., and Reimer, R.W., 2020, CALIB 8.2 [WWW program] at http://calib.org, accessed 2020-10-14.

Them, T.R., Schmidt, M.W., Lynch-Stieglitz, J. (2015). Millennial-scale tropical atmospheric and Atlantic Ocean circulation change from the Last Glacial Maximum and Marine Isotope Stage 3. Earth and Planetary Science Letters 427, 47–56.

Ujiié, Y., Garidel-Thoron, T. de, Watanabe, S., Wiebe, P., Vargas, C. de (2010). Coiling dimorphism within a genetic type of the planktonic foraminifer *Globorotalia truncatulinoides*. Marine Micropaleontology 77 (3-4), 145–153.